ELECTROSTATICS AT AQUEOUS INTERFACES AND IN NANOCONFINEMENT

Dissertation zur Erlangung des akademischen Grades
eines Doktors der Naturwissenschaften am
Fachbereich Physik der Freien Universität Berlin

vorgelegt von

PHILIP LOCHE

Berlin, 2021

Philip Loche: *Electrostatics at Aqueous Interfaces and in Nanoconfinement*

ERSTGUTACHTER: Prof. Dr. Roland R. Netz
ZWEITGUTACHTERIN: Prof. Dr. Bettina G. Keller

TAG DER DISPUTATION: 06.12.2021

Do. Or do not. There is no try.

— Yoda

Dedicated to my Family and Friends.

ABSTRACT

Electrostatic phenomena, like lightning in a thunderstorm or a balloon sticking to our hair, are everywhere in our day-to-day life. These phenomena are based on forces exerted by electric charges described by Coulomb's law. Developed for macroscopic objects, Coulomb's law even holds on the nanoscale with astonishing accuracy describing the interactions of atoms, molecules, and ions, the building blocks of all matter. Understanding their behavior is essential for all-natural sciences. One molecule of utmost importance in natural science is water. An exact electrostatic description of liquid water and its interaction with other dissolved molecules or ions is impossible due to the complex structure of the liquid. Therefore, we are usually content with a continuum description by treating water as an unstructured homogenous - dielectric - material, already explaining several phenomena like ion solvation or colloid precipitation. However, it is known that at interfaces the isotropy and homogeneity of the water's dielectric properties break down. In fact, any modification of the dielectric constant at interfaces or in confined space fundamentally influences all electrostatic interactions including equilibria of chemical reactions or particle distributions.

This thesis aims to understand how the electrostatic interactions are modified in aqueous nanosystems and how well a dielectric continuum description performs. The dielectric properties of water and ions are quantified using classical force field atomistic simulations as well as using novel anisotropic linear continuum descriptions. and compared to recent experiments. For an accurate comparison between the simulations and the continuum description we develop a new simulation force field describing the physics of several monovalent ions in water with higher accuracy compared to previous parametrizations. During the subsequent study of the water properties at planar interfaces and in narrow planar channels, we find that dielectric effects differ in perpendicular and parallel surface direction but decay to the bulk value within 1–2 nm away from the surface. This universal scaling exists regardless of the studied surface type. For water-filled carbon nanotubes, we show that the dielectric tensor becomes, due to curvature effects, even more, anisotropic compared to planar systems.

Based on the dielectric properties extracted from our simulations we analytically calculate interactions of charges with surfaces and between other charges in planar and cylindrical geometry on a linear response level applying previously derived solutions of Poisson's equation. Comparing the analytic predictions to explicit simulations we quantify the breakdown of linear response theory at interfaces and reveal that interactions in confinement are drastically enhanced compared to non confined systems. The findings of this work have an impact for the understanding of the transport, adsorption and evaporation properties of atoms, molecules, and ions which is not only relevant in biological systems but also for technical applications like water purification or energy storage.

ZUSAMMENFASSUNG

Elektrostatische Phänomene wie Blitze in einem Gewitter oder ein Luftballon, der an den Haaren haftet, sind uns allgegenwärtig. Diese Erscheinungen beruhen auf Kräften, die durch elektrische Ladungen hervorgerufen und durch das Coulomb Gesetz beschrieben werden. Entwickelt für makroskopische Objekte, gilt dieses Gesetz bis zur Nanoskala und beschreibt dort die Wechselwirkungen zwischen Atomen, Molekülen sowie Ionen, den Bausteinen aller Materie. Das Verhalten dieser Wechselwirkungen zu verstehen, ist essentiell für alle Naturwissenschaften. Ein Molekül von besonderer Bedeutung ist Wasser. Die exakte elektrostatische Beschreibung von flüssigem Wasser und seiner Wechselwirkung mit anderen Molekülen oder Ionen ist aufgrund seiner komplexen Struktur unmöglich. Daher begnügen wir uns meist mit einer Kontinuumsbeschreibung, bei der Wasser als ein unstrukturiertes homogenes - dielektrisches - Material behandelt wird. Diese Vereinfachung erklärt bereits Phänomene wie Solvatation oder Fällung. Es ist jedoch bekannt, dass an Grenzflächen die Isotropie und Homogenität der dielektrischen Eigenschaften von Wasser zusammenbrechen. Die damit verbundene Änderung der Dielektrizitätskonstanten, beinflusst grundsätzlich alle elektrostatischen Wechselwirkungen, mit Einfluss auf die Gleichgewichte von chemischen Reaktionen sowie Teilchenverteilungen.

Diese Dissertation behandelt elektrostatische Wechselwirkungen in wässrigen Nanosystemen und wie gut eine dielektrische Kontinuumsbeschreibung funktioniert. Die dielektrischen Eigenschaften von Wasser und Ionen werden sowohl mit klassischen atomistischen Simulationen als auch mit einer neuartigen anisotropen linearen Kontinuumsbeschreibung quantifiziert und mit aktuellen Experimenten verglichen. Für einen genauen Vergleich zwischen den Simulationen und der Kontinuumsbeschreibung entwickeln wir ein neues Simulationskraftfeld, das die Physik von einwertigen Ionen in Wasser mit höherer Genauigkeit im Vergleich zu früheren Parametrisierungen beschreibt. Bei der anschließenden Untersuchung der Wassereigenschaften an planaren Grenzflächen und in nanometer großen planaren Poren finden wir, dass unterschiedliche dielektrische Eigenschaften in senkrechter und parallelen Richtung zu der Oberfläche vorherrschen. Diese Anisotropie verschwindet aber innerhalb von 1 bis 2 nm von der Oberfläche, unabhängig vom untersuchten Oberflächentyp. Weiterhin zeigen wir, dass für wassergefüllte Kohlenstoff-Nanoröhren der dielektrische Tensor aufgrund von Krümmungseffekten sogar noch anisotroper wird als im Vergleich zu planaren Systemen.

Basierend auf den aus unseren Simulationen extrahierten dielektrischen Eigenschaften berechnen wir analytisch mit linearer Antworttheorie die Wechselwirkungen von Ladungen mit Oberflächen und mit anderen Ladungen in planarer und zylindrischer Geometrie unter Zuhilfenahme von bereits bekannten Lösungen der Poisson Gleichung. Durch den Vergleich der analytischen Vorhersagen mit expliziten Simulationen quantifizieren wir den Zusammenbruch der linearen Antworttheorie an Grenzflächen und zeigen, dass die Wechselwirkungen in Nanosystemen im Vergleich zu nicht-begrenzten Systemen drastisch erhöht sind. Die Ergebnisse dieser Arbeit haben Auswirkungen auf das Verständnis der Transport-, Adsorptions- und Verdampfungseigenschaften von Atomen, Molekülen sowie Ionen, was nicht nur für biologische Systeme, sondern auch für technische Anwendungen wie Wasseraufbereitung oder Energiespeicherung relevant ist.

LIST OF PUBLICATIONS

This cumulative thesis contains the following first-author publications:

- Philip Loche, Patrick Steinbrunner, Sean Friedowitz, Roland R. Netz, and Douwe Jan Bonthuis. « Transferable Ion Force Fields in Water from a Simultaneous Optimization of Ion Solvation and Ion–Ion Interaction. » In: *The Journal of Physical Chemistry B* (2021). DOI: 10.1021/acs.jpcb.1c05303.
- Philip Loche, Cihan Ayaz, Amanuel Wolde-Kidan, Alexander Schlaich, and Roland R. Netz. « Universal and Nonuniversal Aspects of Electrostatics in Aqueous Nanoconfinement. » In: *The Journal of Physical Chemistry B* (2020). DOI: 10.1021/acs.jpcb.0c01967.
- Philip Loche, Cihan Ayaz, Alexander Schlaich, Yuki Uematsu, and Roland R. Netz. « Giant Axial Dielectric Response in Water-Filled Nanotubes and Effective Electrostatic Ion–Ion Interactions from a Tensorial Dielectric Model. » In: *The Journal of Physical Chemistry B* (2019). DOI: 10.1021/acs.jpcb.9b09269.
- Philip Loche, Cihan Ayaz, Alexander Schlaich, Douwe Jan Bonthuis, and Roland R. Netz. « Breakdown of Linear Dielectric Theory for the Interaction between Hydrated Ions and Graphene. » In: *The Journal of Physical Chemistry Letters* (2018). DOI: 10.1021/acs.jpclett.8b02473.

Furthermore, during the completion of this doctoral research, the following other works were produced:

- Philip Loche, Roland R Netz, and Douwe J Bonthuis. « Evaporation of Nano-Hydrated Ions from Aqueous Solution. » In: (2021).
- Grazia Gonella et al. « Water at Charged Interfaces. » In: *Nature Reviews Chemistry* (2021). DOI: 10.1038/s41570-021-00293-2.
- Majid Rezaei, Bernhard G. Mitterwallner, Philip Loche, Yuki Uematsu, Roland R. Netz, and Douwe Jan Bonthuis. « Interfacial, Electroviscous, and Nonlinear Dielectric Effects on Electrokinetics at Highly Charged Surfaces. » In: *The Journal of Physical Chemistry B* (2021). DOI: 10.1021/acs.jpcb.0c11280.
- Lorena Ruiz-Rodriguez, Philip Loche, Lise Thornfeldt Hansen, Roland R. Netz, Peter Fratzl, Emanuel Schneck, Kerstin G. Blank, and Luca Bertinetti. « Sequence-Specific Response of Collagen-Mimetic Peptides to Osmotic Pressure. » In: *MRS Bulletin* (2021). DOI: 10.1557/s43577-021-00138-9.
- Matej Kanduč, Emanuel Schneck, Philip Loche, Steven Jansen, H. Jochen Schenk, and Roland R. Netz. « Cavitation in Lipid Bilayers Poses Strict Negative Pressure Stability Limit in Biological Liquids. » In: *Proceedings of the National Academy of Sciences* (2020). DOI: 10.1073/pnas.1917195117.
- Hossam Elgabarty, Tobias Kampfrath, Douwe Jan Bonthuis, Vasileios Balos, Naveen Kumar Kaliannan, Philip Loche, Roland R. Netz, Martin Wolf, Thomas D. Kühne, and Mohsen Sajadi. « Energy Transfer within the Hydrogen Bonding Network of Water Following Resonant Terahertz Excitation. » In: *Science Advances* (2020). DOI: 10.1126/sciadv.aay7074.

- Alexandre P. dos Santos, Yuki Uematsu, Alexander Rathert, Philip Loche, and Roland R. Netz. « Consistent Description of Ion-Specificity in Bulk and at Interfaces by Solvent Implicit Simulations and Mean-Field Theory. » In: *The Journal of Chemical Physics* (2020). DOI: 10.1063/5.0016103.
- Shane Carlson, Florian N. Brünig, Philip Loche, Douwe Jan Bonthuis, and Roland R. Netz. « Exploring the Absorption Spectrum of Simulated Water from MHz to Infrared. » In: *The Journal of Physical Chemistry A* (2020). DOI: 10.1021/acs.jpca.0c04063.
- Amanuel Wolde-Kidan, Quoc Dat Pham, Alexander Schlaich, Philip Loche, Emma Sparr, Roland R. Netz, and Emanuel Schneck. « Influence of Polar Co-Solutes and Salt on the Hydration of Lipid Membranes. » In: *Physical Chemistry Chemical Physics* (2019). DOI: 10.1039/C9CP01953G.
- Philip Loche, Amanuel Wolde-Kidan, Alexander Schlaich, Douwe Jan Bonthuis, and Roland R. Netz. « Comment on "Hydrophobic Surface Enhances Electrostatic Interaction in Water". » In: *Physical Review Letters* (2019). DOI: 10.1103/PhysRevLett.123.049601.

CONTENTS

1 INTRODUCTION 1

2 THEORETICAL FRAMEWORK 5
- 2.1 Linear Dielectric Theory 5
- 2.2 Solvation Energy 7
- 2.3 The Method of Image Charges 8
- 2.4 Dielectric Profiles 9
- 2.5 Principles of Classical Molecular Dynamics Simulations 10

3 DEVELOPMENT OF AN ION FORCE FIELD 13

4 ELECTROSTATICS OF PLANAR NANO SYSTEMS 23

5 ELECTROSTATICS OF CYLINDRICAL NANO SYSTEMS 33

6 LIMITS OF LINEAR ELECTROSTATICS 43

7 CONCLUSION 51

8 OUTLOOK 53

BIBLIOGRAPHY 55

1 INTRODUCTION

Life as we know it is based on cells which are the smallest building blocks of biological organisms. However, cells are not the smallest building block that we know of. Their organelles are made out of molecules, that themselves consist of sometimes up to a few hundred thousands atoms. Therefore, quantifying the interactions between atoms and molecules is essential to understand the mechanisms inside and between cells and is important for a better understanding of life. On a fundamental level, we know that interactions, including those between atoms, can be divided into four classes, also known as the four fundamental forces. These forces are fundamental, since, to our best knowledge, they are not reducible to more basic interactions. These four forces are the gravitational, electromagnetic, strong, and weak interaction. The latter two play a major role in subatomic distances. For our everyday life, naively, we would give gravity the biggest role. Gravitation takes care that our dishes do not float around in our rooms and is responsible if one plate is painfully dropping on our foot. Yet, the gravitational force is the weakest of all fundamental forces. This fact can be easily demonstrated by levitating or hovering objects. For example, a magnet can hover above a superconductor held only by the electromagnetic force. The gravitational force between the magnet and the whole earth is compensated for by the superconductor weighting only a few grams. A more mathematical explanation is given by calculating the ratio of electrostatic and gravitational force between two charged objects. The electrostatic force is also known as Coulomb's force named after its most prominent researcher Charles Augustin de Coulomb, who lived at the end of the 18th century. Gravity and the Coulomb force decay proportional to the distance between charges and the ratio of the two forces only depends on physical constants. One finds that the electrostatic repulsion between two electrons is $4.2 \cdot 10^{42}$ times larger than their gravitational attraction. Due to this fact the most important interaction between atoms and molecules are of electrostatic nature[1].

Electrostatic interactions therefore also are playing a major role in the interactions between water and other substances. All living organisms need water to retain their metabolism and water is also the main constituent of Earth's hydrosphere. The molecule, made of two hydrogens and one oxygen atom, is one of the most studied materials. The academic interest is not only because of its importance to life and its ubiquity on earth, but also due to its remarkable properties as an exceptional liquid. On the macroscopic scale (meters down to micrometers), many experiments and theories have been developed over the last centuries that explain its properties [1]. But below the scale of micrometers, the study of fluids is still of great interest. Biologically and technologically relevant is the investigation of fluids close to surfaces or confined between surfaces. Generally, confining a fluid to a structure scaling from 1-100 nanometer induces large changes in the physical

1 Even though electrostatic is far stronger than gravity, electrostatic interaction is on larger length scales negligible. This originates simply because macroscopic bodies contain equal numbers of positive and negative charges resulting in no net electric charge and therefore no repulsion or attraction. However, for gravity, there is not such cancellation and it is always attractive.

behavior because characteristic length scales are in the same order of magnitude as the size of the confinement. Examples are the Bjerrum length, the distance at which electrostatic interactions decay to k_BT, the Debye screening length, also a measure how far electrostatic effects persist, or the slip length. The slip length defined as the ratio of the stress and the shear rate quantifies how much « lubricant » viscous fluids have at solid boundaries. One observed effect in confinement connected to the slip length is an increased permeability of confined water, which is 10^3 times higher than predicted by classical fluid theories [2]. It is also generally acknowledged that changed water properties at interfaces or in confinement significantly modify surface interactions, ionic adsorption, and molecular transport [3–13]. Confined liquids also change the equilibria of chemical reactions like the protonation/deprotonation equilibria of acids. However, the precise mechanisms behind the changed properties of confined and the consequences for dissolved particles are not clear.

In the last decades novel assembly methods allowed to build nanometer cavities filled with water. For planar pores, also known as nano slits, the van der Waals assembly of two-dimensional materials allows the creation of artificial channels with sub-nanometer precision [2, 14–22]. This remarkable assembly method allows to build devices with a wide range of applications, such as graphene-based water purification [23], double-layer capacitance [24] osmotic power harvesting [25] and electrowetting [26], as well as for biological functions, such as molecular recognition [27] and DNA condensation [28]. For cylindrical nanopores so-called Nanojet systems allow measuring the pressure-driven flow of water and other molecules through individual carbon nanotubes or boron nitride nanotubes with well-defined radii down to a few tenths of a nanometer [29, 30]. Fluids in cylindrical cavities can also be used as an analogy for electronic components such as signal multipliers [31], diodes [32] or even transistors [33]. Progress in the field could also help to understand the efficiency of biological nanopores. For example, aquaporin channels are a key component in many biological processes and play the role of water filters in biological membranes [34, 35]. They are permeable for water molecules but very selective for other molecules [36]. There are also biological proton pumps, membrane proteins that drive protons against electrochemical gradients [37]. Here, electrostatic effects decisively control the effective proton mobility in protein channels and close to surfaces, in addition to the water occupancy in channels and the configuration of flanking amino-acid groups [38, 39]. Artificial nanopores can act as semipermeable membranes for water desalination using reverse osmosis [40, 41] or as gas storage [42].

To understand the occurring effects and promote the development in the growing field of wet nanoscience, besides sophisticated experimental techniques, suitable theoretical frameworks in combination with powerful simulation methods are necessary. State of the art classical molecular dynamics (MD) simulations can calculate the motion of ten or even a hundred thousand of atoms and are the method of choice for interfacial and confined systems [43]. Other common simulation techniques are Monte Carlo (MC) or quantum chemical simulations from first principals, called ab-initio (AIMD) simulations. MC simulations miss any dynamics of the system and a treatment of the complex water structure is usually hard [44]. In standard Born-Oppenheimer AIMD simulations the evaluation of the forces acting on each nucleus requires a calculation of the electronic ground (or excited) state energy and its derivatives with respect to the nuclear positions at each MD step compared to classical simulations where quantum effects are approximated by

empirical potentials, called force fields. The advantage of AIMD, however, comes with enormous computational costs. AIMD simulations are orders of magnitude more computationally expensive compared to classical MD simulations. Besides, appearing quantum effects can be handled with reasonable accuracy implicitly using rigorously parametrized force fields[2] which is one crucial parameter in classical simulations. Especially, for ion force fields, there has been a fierce and ongoing debate about how to properly design a classical one [45–47] and currently no parametrization exists that covers a wide range of ions.

Besides numerical analyses, analytical theories are applied to explain appearing phenomena on the nanoscale. As all atomic interactions originate from charges their mathematical description is based on Maxwell's equations. Maxwell's equations formulated in the 19th century are a well-known and established theory. The equations can explain many of our all-day phenomena like friction, the blue sky, or lightning. Maxwell's equations are also the fundamental theory behind all digital devices like television or computers either on our tables or in our pockets. One part of Maxwells' theory is explaining how charges interact with each other when not in motion. On the nanoscale Coulumb's law, a solution of Maxwell's equation still holds with astonishing accuracy. Yet, deducing exact theories based on Coulomb's law is often analytically not feasible due to a large number of involved particles. An approximation is to treat all solvent particles implicitly as a linear dielectric medium. This approximation works well in bulk systems even though it ignores the structure of the solvent. At interfaces and in confinement with length scales below 1 nm it is not clear if this linear approximation is valid, since the length scale is on the order of typical solvent molecules like water. However, continuum models like the Navier-Stokes (NS), the Poisson–Boltzmann (PB), or the Poisson-Nernst-Planck (PNP) equation are applied to describe the properties and the transport of ionic and non-ionic liquids in narrow pores. It is remarkable that for example the NS equation, developed in the 19th century, is still valid in nano-channels with diameters of 1–2 nanometers [2]. However, for a realistic description of ionic transport using the PNP equation or for calculating the interactions and distributions of ions in a liquid using the PB equation, a well-founded description of the liquid's dielectric properties are indispensable.

Even though, interfacial water was very early shown to have a reduced dielectric constant compared to bulk [48], in most contemporary modeling approaches, water is treated as a linear dielectric and its permittivity at interfaces and in confinement is assumed to be isotropic and given by the dielectric constant of bulk water. A simplified treatment of the water structure could cause discrepancies between experimental observables and some theoretical predictions [49, 50]. If anisotropic effects on a linear level are included correctly it was shown that this has significant effects on surface capacitances, Zeta potentials, and surface conductivities [51]. Recent experiments in the Geim group [24] in agreement with prior simulations [52] demonstrated a significant change of the dielectric properties for water confined in planar nano slits. But how dielectric properties in confinement translate to electrostatic interactions and how surface properties (soft/hard, non-polar/polar) influence the dielectric response of confined water has remained unclear. Even though, the equations for electrostatic interactions in planar and cylindrical geome-

2 Only when the translational or rotational motion of light atoms (He, H, D) with vibration frequencies with energies higher than k_BT, are studied, one should think about adding explicit quantum effects of nuclear motions

try already have been derived [53], currently no data for the permittivity, the crucial input parameter for analytical modeling, exists. Additionally, there always arises the question: How reliable is a linear dielectric theory? It was shown that linear response is valid for monovalent ions in water but breaks down for multivalent ions [54]. At interfaces and confinement, currently, no study exists investigating the possible breakdown of linear response theory which requires extensive computer simulations due to the complex structure of water.

The presented work is divided into five parts. In the next chapter the scientific background and theoretical frameworks are presented that are important for investigating electrostatics in solutions. In chapter 3 we present the development of a new force field necessary to simulate ions in water. Afterwards, in chapters 4 and 5 the dielectric properties in planar nano slits and cylindrical nanopores are presented. Chapter 6, investigates electrostatic effects of ions at aqueous interfaces based on simulations and analytical modeling. Finally, the conclusions and an outlook is formulated (chapter 7).

2 THEORETICAL FRAMEWORK

In this chapter, we lay out the theoretical framework and the simulation techniques required to handle electrostatics on the nanoscale, starting by introducing linear dielectric theory.

2.1 LINEAR DIELECTRIC THEORY

In the simplest electrostatic theory, charges are assumed to be point-like and embedded in a medium where the water molecules are treated as a structureless, linear dielectric medium. Generally, without a dielectric medium, interactions between charges are calculated based on Gauß's law for electrostatics, a part of Maxwell's equations

$$\boldsymbol{\nabla} \cdot \boldsymbol{E}(\boldsymbol{r}) = \frac{\rho(\boldsymbol{r})}{\varepsilon_0} \,, \tag{2.1}$$

where $\boldsymbol{E}$ is the electric field, ε_0 the vacuum permittivity and $\rho(\boldsymbol{r})$ the charge density. The electric field is proportional to the total force $\boldsymbol{F}$ on a charge q (in terms of the elementary charge e) since $\boldsymbol{F}(\boldsymbol{r}) = qe \cdot \boldsymbol{E}(\boldsymbol{r})$. Solving eq. (2.1) equation for two point like objects one recovers the potential energy between two charges 1, 2 in vacuum, Coulomb's law,

$$\frac{U_{\mathrm{Coul}}^{\mathrm{vac}}}{k_{\mathrm{B}}T} = \frac{q_1 q_2 e^2}{4\pi\varepsilon_0 k_{\mathrm{B}} T |\boldsymbol{r}_1 - \boldsymbol{r}_2|} = \frac{q_1 q_2 l_{\mathrm{B}}^{\mathrm{vac}}}{|\boldsymbol{r}_1 - \boldsymbol{r}_2|} \,, \tag{2.2}$$

where k_{B} is the Boltzman constant and T the Temperature. q is the charge in terms of the elementary charge e and $\boldsymbol{r}$ its position. Eq. (2.2) alo introduces the Bjerrum length in vacuum $l_{\mathrm{B}}^{\mathrm{vac}}$ which is the distance where the electrostatic interaction between two elementary charges equals $k_{\mathrm{B}}T$. The Bjerrum length at room temperature in vacuum is ~ 60 nm, showing that the Coulomb potential is a strong long-range interaction. In eq. (2.2), all charges are taken explicitly into account (Fig. 2.1). Neglecting the structure of all net-uncharged but polar molecules, like water, the fundamental equation for describing interactions between charges, Gauß's law in matter, is modified to

$$\nabla \cdot \boldsymbol{D}(\boldsymbol{r}) = \rho_{\mathrm{f}}(\boldsymbol{r}), \tag{2.3}$$

where ρ_{f} is the charge density of free charges (ions, charged molecules, or surfaces) and $\boldsymbol{D}$ is a vector field called displacement field

$$\boldsymbol{D} = \boldsymbol{P} + \varepsilon_0 \boldsymbol{E} \,. \tag{2.4}$$

The field is called displacement field, because charges are displaced by the alignment of dipoles or the deformation of electron clouds. $\boldsymbol{P}$ is the polarization, a vector field describing the density of permanent or induced electric dipole moments. These dipole moments could be created by the alignment of a water molecule due to an electric field created by other water molecules in its vicinity. However, the

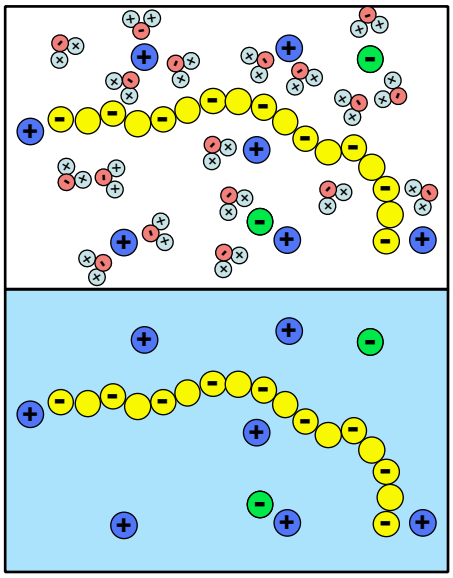

Figure 2.1: Sketch of a charged chain surrounded by water molecules and ions (upper). Interactions are described by eq. (2.2). The same system using an implicit solvent with an increased effective permittivity. Interactions are described by eq. (2.5) (lower).

explicit functional relation between the electric field $\boldsymbol{E}$ and the polarization $\boldsymbol{P}$ is complex and depends on the specific material. For small fields, the polarization can be expanded in a Taylor series as a function of the electric field $\boldsymbol{P}(\boldsymbol{r}) = \varepsilon_0 \chi \boldsymbol{E}(\boldsymbol{r}) + \dots$ where the proportionality constant $\chi = \varepsilon - 1$ is called the susceptibility. The dots indicate higher non linear orders for the relation, between the polarization and the electric field. Following the linear relation the displacement field is proportional to the electric field $\boldsymbol{D}(\boldsymbol{r}) = \varepsilon\varepsilon_0 \boldsymbol{E}(\boldsymbol{r}) + \dots$ and Coulomb's equation in matter is recovered

$$\frac{U_{\text{Coul}}}{k_{\text{B}}T} = \frac{q_1 q_2 e^2}{4\pi\varepsilon_0 \varepsilon k_{\text{B}} T |\boldsymbol{r}_1 - \boldsymbol{r}_2|} = \frac{q_1 q_2 l_{\text{B}}}{|\boldsymbol{r}_1 - \boldsymbol{r}_2|} \,. \tag{2.5}$$

Here ε is the dielectric constant or permittivity of the medium and l_{B} the Bjerrum length. The consequences of eq. (2.5) is sketched in the lower panel of Fig. 2.1. The permittivity is a measure of the resistance that evolves when electric fields are formed in matter. In simple words, it indicates how electric fields are guided and if they are weakened compared to vacuum. For example, in water, which has a relative dielectric constant of around 80, the strength of electric fields is reduced down to approximately 1%. Consequently, the Bjerrum length also reduces to ~ 0.8 nm, reducing the length of the significant interaction in water compared to vacuum by more than an order of magnitude. As shown below, the electric permittivity also undergoes large changes, when a fluid is confined. The large permittivity of water arises from the high molecular polarity of the molecules. One can estimate the dielectric constant ε for a single molecule by calculating its average polarization along one direction caused by an electric field E [52]. The dielectric constant for a non-interacting single molecule follows from the Langmuir model [55] as $\varepsilon = 1 + np^2/(3\varepsilon_0 k_{\text{B}} T)$. For a water number density $n \approx 33\,\text{nm}^{-3}$ and a water dipole moment of $p = 0.05\,\text{e}\cdot\text{nm}$ the resulting dielectric constant is $\varepsilon = 20$ – a large reduction of electrostatic interactions due to water dipole orientation but is much smaller than the experimental value. The discrepancy can be explained by

collective effects since the experimental value is roughly 4 times higher. This a crude definition of the Kirkwood g factor [56, 57]

$$\varepsilon = 1 + \frac{(n/g)\,(pg)^2}{3\varepsilon_0 k_\mathrm{B} T}\,. \tag{2.6}$$

In conclusion, the dielectric constant of water reduces interactions of charges and is dominated by collective effects where ¼ comes from the « self contribution » ¾ from « collective contribution ». We will now estimate the energy necessary to create a charge distribution inside a dielectric environment.

2.2 SOLVATION ENERGY

Solvation describes the interaction of the solvent, for example water, with dissolved molecules, the solutes. Depending on the type of a solute the contribution to the energy is either negative or positive. For uncharged (hydrophobic) molecules, like alkanes, the solvation energy in water is positive. Hydrophobic molecules disturb the hydrogen bond network in an unfavorable manner. In contrast, polar or charged molecules, like ions, are hydrophilic since they fit into the hydrogen bond network and their solvation energy therefore is negative and energy is released when they are solvated.

Considering only the electrostatic/Coulomb contribution of solvation the energy F_Coul of creating a solute with the charge density $\rho(\boldsymbol{r})$ inside an environment of already existing charges is

$$F_\mathrm{Coul} = \frac{1}{2}\iint \rho(\mathbf{r})\mathcal{G}(\mathbf{r},\mathbf{r}')\rho(\mathbf{r}')\mathrm{d}\mathbf{r}\,\mathrm{d}\mathbf{r}'\,. \tag{2.7}$$

From a mathematical point of view, the goal is to find Green's function $\mathcal{G}$ that follows from Poisson's equation

$$\Delta\cdot\mathcal{G}(\mathbf{r},\mathbf{r}') = -\frac{\delta(\mathbf{r}-\mathbf{r}')}{\varepsilon_0\varepsilon}\,. \tag{2.8}$$

The Green's function is the electrostatic potential due to a unit source and its image charges (see below). In $\mathcal{G}(\mathbf{r},\mathbf{r}')$, the vector $\mathbf{r}'$ refers to the location of a unit source, and $\mathbf{r}$ is the point at which the potential is being evaluated [58]. Poisson's equation follows from Gauß's law as easily verified by taking the derivative eq. (2.1). Due to the complex structure of liquids, finding the solution of a general Green's function (as for example introduced in section 2.3) is typically not accessible analytically. However, the integral in eq. (2.7) is trivially solvable, as it uses an implicit solvent approximation, introduced in section 2.1. At first shown by Born [59] in his work « Volumen und Hydratationswärme der Ionen » the solvation energy difference for a spherical charged shell of radius a brought from the air phase ($\varepsilon = 1$) into a solvent with a certain dielectric constant is

$$F_\mathrm{Coul} = \frac{q^2}{8\pi\varepsilon_0 a}\left(\frac{1}{\varepsilon}-1\right). \tag{2.9}$$

The Born equation accurately reproduces the solvation energy of many ions, as shown in Fig. 2.2, even though it neglects the water structure and with this non linear effects, as well as non electrostatic effects. The reason, why nevertheless a good agreement with experiment exists, is explained in chapter 6.

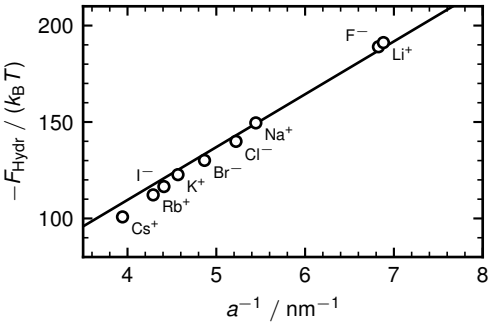

Figure 2.2: Negative energy of hydration of different ions as function of their inverse crystal radius a [60]. The straight line represents the Born equation given in eq. (2.9).

The solvation refers to the process of adding one solute to an infinite diluted system. For adding one particle to a system at finite concentration one generalizes the concept and introduces the chemical potential

$$\mu = \mu_0 + k_{\mathrm{B}}T \ln(\gamma_x), \tag{2.10}$$

where μ_0 is the chemical potential at zero concentration; the solvation free energy. Further x is the mole fraction and γ_x the activity coefficient which may itself depend on x. The mole fraction is the amount of solutes (expressed in moles) divided by the total amount of all particles in a mixture. The activity coefficient describes deviations from the ideal behavior of specific mixtures. An ideal mixture or an ideal solution exhibits the same thermodynamic properties as mixtures of ideal gases. Especially no heat is released nor the volume is changed when two particle types are mixed.

2.3 THE METHOD OF IMAGE CHARGES

So far, only solutes in bulk solutions were considered. In bulk, solutes do equally distribute over the whole space. At interfaces, the solute distribution becomes inhomogeneous because of solute-interface interactions. One of the simplest electrostatic theories to model the interaction of charges at interfaces is the method of image charges. Suppose a point charge q is held at distance d in front of an infinite grounded conducting plane. The potential is not the standard Coulomb force directly obtained from eq. (2.2) since the charge will induce a counter charge q' on the surface. Again, one has to solve eq. (2.7). However, for the constituent equation for Green's function now contains a position dependant permittivity

$$\varepsilon_0 \left\{ \nabla \cdot \left[\boldsymbol{\varepsilon}(\mathbf{r}) \cdot \nabla \mathcal{G}(\mathbf{r}, \mathbf{r}') \right] \right\} = -\delta(\mathbf{r} - \mathbf{r}') \,. \tag{2.11}$$

The Green's function has to fulfill the boundary conditions that first $\mathcal{G}(\mathbf{0}, \mathbf{r}') = 0$ when the observer is at the interface (since the conducting plane is grounded) and second, the standard Coulomb law is recovered for large distances from the interface. It turns out [61] that this problem is equivalent to putting a second point charge with an opposite sign at $-d$. For a general dielectric interface (panel 1–3 in Fig. 2.3) eq. (2.7) for $d > 0$ is [58]

$$F_{\mathrm{Coul}}(d) = \frac{q^2}{8\pi\varepsilon_0\varepsilon} \left(\frac{1}{a} + \frac{\lambda}{2d} \right), \tag{2.12}$$

where λ is the dielectric contrast. For metal surfaces $\lambda = -1$ so that the charge and its image are of different sign, but for general permittivities one finds $\lambda =$

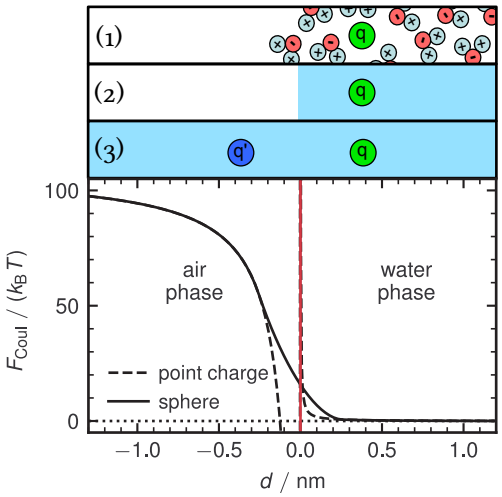

Figure 2.3: Sketch of the image charge model for a point charge (upper three panels): (1) all charges are treated explicitly. (2) implicit solvent approximation (3) mathematically equivalent problem. The lowest panel shows the image charge potential for a point charge and the solution of the electrostatic problem for a charged spherical shell.

$(\varepsilon_1-\varepsilon_2)/(\varepsilon_1+\varepsilon_2)$ [58]. If the charge is placed inside the stronger dielectric one finds that $q' = \lambda q$ is positive and otherwise negative. For water ($\varepsilon_1 = 80$) and vacuum ($\varepsilon_2 = 1$) one finds that the dielectric contrast is ≈ 0.97 so that the charge and its image repel each other. Equation (2.12) is the basis of many theories including the theory of Onsager and Samaras [62] explaining the surface tension increase of electrolyte solutions as a function of concentration. However, eq. (2.12) shows that at interfaces the resulting image charge repulsion diverges inversely with the ion-interface separation (Fig. 2.3), suggesting that ions can never cross any dielectric interface even if the dielectric contrast λ is infinitely small. This nonphysical result can be corrected if ions are not treated as point charges but as finite spheres, as first rigorously demonstrated by Tamashiro and Constantino [63]. They treated an ion as a sphere with radius a and surface charge density $\sigma = q/4\pi a^2$, yielding a smooth potential. As the electrostatic problem becomes more intricate, the image charge method is not applicable anymore directly if the charge penetrates into the surface. The problem solved by Tamashiro and Constantino is generalized for a second interface parallel to the first one in Chapter 4. A second interface leads to an infinite series of images charges « mirrored » at both interfaces. Additionally, the method is also applicable for a charge inside a cylindrical interface (see Chapter 5). However, as presented in the next section, permittivities are not sharp box like functions, as assumed here. At interfaces, permittivities vary similar as a function of the position.

2.4 DIELECTRIC PROFILES

Simulations revealed that at interfaces [64], around solutes [65] or in planar confinement [52, 66] the dielectric constant changes drastically. In the vicinity of surfaces, the permittivity is not a scalar anymore but a tensor, whose structure depends on the explicit geometry. Its entries can be obtained from the fluctuations of the polarization even without applying an external finite field. This method was developed by John G. Kirkwood and Fröhlich [57] in 1939 and first applied to simulations in 1983 by Neumann [67]. Although the technique for deriving the fluctuation formulas are known for almost 40 years, a careful application of the electrostatic boundary condition is necessary, which led to several controversies [68–70]. A simple test of the correctness of the derivation is to compare the predicted electric fields with

the electric field found in separate simulations where a constant displacement field has been applied. The test for a graphene-water interface is further discussed in chapter 4.

Here, exemplarily the derivation for planar dielectric profiles is sketched. The relation between the dielectric constant and the fluctuations of the polarization depends on the geometry and the electrostatic boundary conditions of the system under consideration, but it always boils down to the general non-local response relation [52, 64, 71].

$$\boldsymbol{D}(\boldsymbol{r}) = \varepsilon_0 \int \mathrm{d}\boldsymbol{r}' \hat{\varepsilon}_{\mathrm{nl}}(\boldsymbol{r}, \boldsymbol{r}') \boldsymbol{E}(\boldsymbol{r}, \boldsymbol{r}'), \tag{2.13}$$

where $\hat{\varepsilon}_{\mathrm{nl}}(\boldsymbol{r}, \boldsymbol{r}')$ is an anisotropic but diagonal non local dielectric tensor. At infinite planar interfaces, pointing along the z direction and being isotropic in the other two directions, applying the Maxwell–Faraday equation

$$\boldsymbol{\nabla} \times \boldsymbol{E}(\boldsymbol{r}) = \boldsymbol{0}\,,$$

leads to the fact that the parallel (xy) component of the electric field $E_\parallel$ is constant. Consequently, eq. (2.13) simplifies to $D_\parallel(z) = \varepsilon_0 \varepsilon_\parallel(z) E_\parallel(z)$, where $\varepsilon_\parallel(z) = \int \mathrm{d}z' \hat{\varepsilon}_{\parallel,\mathrm{nl}}(z, z')$ is the local dielectric profile. Applying eq. (2.4) the parallel dielectric profile a solution can be obtained to extract dielectric profiles from atomistic simulations [52, 64, 71].

As stated in this section, dielectric profiles are extracted from simulations. In the last section of this chapter, a brief introduction to the principles of classical molecular dynamics Simulations is given.

2.5 PRINCIPLES OF CLASSICAL MOLECULAR DYNAMICS SIMULATIONS

As stated several times above, the analytical treatment of Coulomb forces beyond the linear level is usually not feasible for many particle systems. However, to extract dielectric profiles and test linear approximations, model-free methods are necessary that treat the interaction of charges beyond the linear level. Molecular Dynamics (MD) simulations are a technique to calculate the properties of N-body systems using the classical laws of mechanics. They especially allow calculating Coulomb forces exactly by solving Poisson's equation, given in eq. (2.8), numerically with high accuracy. The general algorithm works as follows:

1. Set the initial conditions of the system, such as positions and velocities.
2. Based on the positions the forces are calculated using parametrized energy function, called force fields.
3. Newton's equation of motions is integrated leading to new positions.

Steps two and three are calculated several times creating so called trajectories of the particles. A key part of MD is the force field that has to cover all pairwise interactions, which arise from quantum mechanics and electrostatics. While these force fields neglect chemical reactions, they are able to reproduce many observables like distribution functions, surface potentials and even dynamic processes for trajectory lengths that cannot be covered by quantum simulations. Three common force field

parametrization are the Groningen Molecular Simulation (GROMOS) set [72], the Assisted Model Building with Energy Refinement (AMBER) [73] or the Chemistry at Harvard Macromolecular Mechanics (CHARMM) [74]. Since all dynamics depend on the force field parameters, it is indispensable to determine them with extreme care, for example by deducing them from experimental studies. Wrong parameters inevitably lead to wrong observations. Force fields can be arbitrarily complicated but most of these energy functions are split into *bonded* and *non-bonded* interactions. As the name suggests bonded interactions describe the structure of bonds. This also includes the correct bond angles between three atoms and dihedrals, the angle spanned between planes through two sets of three atoms. Usually, the potentials for bonds, angles, and dihedrals are harmonic. Non-bonded interactions describe Van-der-Waals attraction, steric repulsion, and Coulomb interactions. The first two are combined into a so called Lennard-Jones potential

$$U_{\mathrm{LJ}}(r) = 4\epsilon \left[\left(\frac{\sigma}{r}\right)^{12} - \left(\frac{\sigma}{r}\right)^{6} \right]. \tag{2.14}$$

Here ϵ is the strength of the potential and σ the distance, where the potential vanishes. Note that the first mimics steric repulsions and the second term models the Van der Waals attraction. The exponent of the first term is chosen in such a way that it is the square of the second term. This is an arbitrary choice but optimizes the runtime.

For simulation only containing one type of particles, like noble gases, only one pair of parameters is necessary: one Lennard-Jones radius σ and one Lennard-Jones energy ϵ. Adding a second particle type, the number of parameter pairs increases to three: two for the interaction between particles of the same kind and one for the interaction between the two. The number of parameter pairs for a system containing N particle types is $N(N+1)/2$. One could imagine that the interaction of two dissimilar non-bonded atoms could be deduced by combining the interaction of atoms of the same kind. This would reduce the number of independent parameters. One possible so called mixing or combination rule was developed by Lorentz [75] and Bertelot [76]

$$\sigma_{ij} = \frac{1}{2}(\sigma_i + \sigma_j) \qquad\qquad \epsilon_{ij} = \sqrt{\epsilon_i \epsilon_j}\,,$$

where i and j are different particle types. If mixing rules are applied, the number of independent parameter pairs reduces to N. The arithmetic average of Lennard Jones radii is only exact for hard spheres and the geometric average of the interaction strengths is also only an approximation. Therefore, there is no guarantee that these combinations give accurate results. In fact, most force fields use a mixture of Lennard-Jones parameters from mixing rules and explicit interaction between particle types.

Besides the Lennard-Jones interaction, the second part of non-bonded interactions is the implementation of Coulomb forces as given in eq. (2.2), utilizing parametrized atomic (partial)-charges. These partial charges are fixed during the whole simulation and therefore do not allow for explicit atomic polarization. However, implicit atomic polarization can be included by choosing the Lennard-Jones parameters accordingly [77] and molecular polarizability is included with flexible molecules.

The calculation of forces is the most time-consuming part of the simulation. In large systems, as also covered in this thesis, with more than 10^4 particles, it is crucial to avoid the computation of all particle pair interactions since they scale

quadratically ($\mathcal{O}(N^2)$). Lennard-Jones interactions decay with r^{-6}, therefore a simple truncation with an analytic tail correction is acceptable. Electrostatics have a long-range $1/r$ decaying tail (see eq. (2.2)). A simple cut-off leads to wrong results even for very simple systems, like a pure dipolar liquid [67]. Today's method of choice dates back to the early 20th century and to Paul Peter Ewald, a German physicist, who worked with x-rays and wanted to calculate electrostatic energies of ionic crystals. His summation technique uses the periodicity of the system to treat the problematic long range tail by using a Fourier summation. Combined with mesh based methods, like fast Fourier transformation (FFT), the computational effort goes down to $\mathcal{O}(N\log N)$ [78, 79].

3

DEVELOPMENT OF AN ION FORCE FIELD

Proper treatment of water and ions is the key to the accurate modeling of both charged and uncharged substances in an aqueous solution. This becomes especially important at interfaces and in confinement where the properties of water change drastically. In classical MD simulations, this comes down to choosing the correct interatomic interaction potential – the force field – for the water and the ions. A physically decent model for water in its condensed phase is SPC/E (Simple Point Charge extended) [80]. The SPC/E model represents water as a triatomic molecule made of oxygen and two hydrogens each rigidly bonded to the oxygen. The bond length between each hydrogen and the oxygen as well as the angle between the bonds is fixed. The triatomic molecule has a single Lennard-Jones site centered on the oxygen atom. A negative point charge is located on the oxygen and two equal positive point charges on the hydrogens. The model is optimized to reproduce the value of the liquid density at room temperature and normal pressure as well as the vaporization enthalpy. Furthermore, it reproduces the water surface tension and the viscosity reasonably well [81] and is used in this thesis. However, the dielectric constant of the SPC/E model is 13% below the experimental value and the temperature dependence of the permittivity is also only poorly reproduced. Even though, SPC/E has these drawbacks it is still the best water model for studying electrostatic properties of aqueous systems containing different solutes. The reason why it is still widely spread in the scientific community originates in the enormous work and the poor academic acknowledgment of new force field developments. Most common force fields are developed and improved over decades and switching the water model usually leads to starting from scratch again since all interactions have to be parametrized again. More recent water models exist, however, they usually only contain force field parameters for water-water interaction and are not tested in conjunction with solutes. Especially the TIP4P/ε (transferable intermolecular potential with 4 points) model [82], reproduce water properties more accurately compared to SPC/E and is therefore preferred to use in future works. The gap of fitting ion interaction parameters are filled by the force field developed in this work. TIP4P/ε model is also a rigid water model, where the Lennard-Jones site and the negative partial charge of the oxygen is slightly shifted against each other. TIP4P/ε is optimized for the experimental dielectric constant and to match the temperature of the maximal density. It reproduces the dielectric constant, thermodynamics, dynamical and structural properties over a wide temperature and pressure range in excellent agreement with experimental data.

For ion force fields, there has been a fierce and ongoing debate about how to properly design a classical one [45–47]. Many existing ion force fields consisting of only Coulomb and Lennard-Jones interactions have been found to produce unreliable results, and claims have been made that different water models require different ion force fields [83–86]. Furthermore, a prevalent assumption has been that the combination of a fixed Coulomb charge and Lennard-Jones interactions cannot be used because of the widely varying dielectric constant in molecular systems. Instead, there have been numerous attempts to introduce polarizability into the interaction potential [87, 88]. A reasonable ion force field for the SPC/E model was

developed by Smith et. al [89, 90]. They optimized their parameters against gas-phase binding enthalpies as well as solvation enthalpies of ionic solutions. Especially the last one is of high importance if electrostatic effects are studied. Smith's force field works well for NaCl and we use their Cl^- parameters for the other chapters. However, Smith's force field, among others, lacks a thorough optimization in the complete parameter space of the Lennard-Jones potential, which is important if more ions should be covered by a force field. The Lennard-Jones potential provides enough freedom to optimize the force field of Na^+, K^+, Cl^-, and Br^- [77, 91–93].

In the current chapter all force field parameters were rigorously fixed by optimizing with respect to the activity coefficient and the solvation free energy only using standard mixing rules. The new force field reproduces the density, conductivity, the dielectric decrement, and the water viscosity as a function of salt concentration with high accuracy. The water self-diffusion coefficient is not reproduced well by our new force field and probably more complex water and ion models might be necessary to capture these kinetic properties. Important conclusions from the optimization procedure include:

1. Despite the large variation of the dielectric constant, the force field performs well up to salt concentrations of at least 5 mol per kg. This shows that the variation of the dielectric environment does not necessitate the introduction of more complex interaction potentials or explicit polarizability, as previously thought.

2. The force field is transferable between the major rigid non-polarizable water models and therefore is directly applicable to more recent models that sufficiently reproduce even more water properties compared to SPC/E.

The work shown in this chapter greatly simplifies the modeling of the aqueous phase in molecular dynamics simulations, removing a persistent source of uncertainty. Furthermore, by using an exact and rigorous method to determine the ion force field parameters, we provide a framework on which further optimizations can be based.

DATA AVAILABILITY

The data that support the findings of this chapter are included in the SI of the publication. The simulations are carried out with the 2019 version of the GROMACS simulation package and analysis are performed with GROMACS and MAICoS. Original simulation and analysis files are available at

http://dx.doi.org/10.17169/refubium-30888.

THE JOURNAL OF PHYSICAL CHEMISTRY B
A JOURNAL OF THE AMERICAN CHEMICAL SOCIETY

pubs.acs.org/JPCB Article

Transferable Ion Force Fields in Water from a Simultaneous Optimization of Ion Solvation and Ion−Ion Interaction

Published as part of The Journal of Physical Chemistry virtual special issue "Dor Ben-Amotz Festschrift".

Philip Loche, Patrick Steinbrunner, Sean Friedowitz, Roland R. Netz, and Douwe Jan Bonthuis*

Cite This: *J. Phys. Chem. B* 2021, 125, 8581−8587 Read Online

ACCESS | Metrics & More | Article Recommendations | Supporting Information

ABSTRACT: The poor performance of many existing nonpolarizable ion force fields is typically blamed on either the lack of explicit polarizability, the absence of charge transfer, or the use of unreduced Coulomb interactions. However, this analysis disregards the large and mostly unexplored parameter range offered by the Lennard-Jones potential. We use a global optimization procedure to develop water-model-transferable force fields for the ions K^+, Na^+, Cl^-, and Br^- in the complete parameter space of all Lennard-Jones interactions using standard mixing rules. No extra-thermodynamic assumption is necessary for the simultaneous optimization of the four ion pairs. After an optimization with respect to the experimental solvation free energy and activity, the force fields reproduce the concentration-dependent density, ionic conductivity, and dielectric constant with high accuracy. The force field is fully transferable between simple point charge/extended and transferable intermolecular potential water models. Our results show that a thermodynamically consistent force field for these ions needs only Lennard-Jones and standard Coulomb interactions.

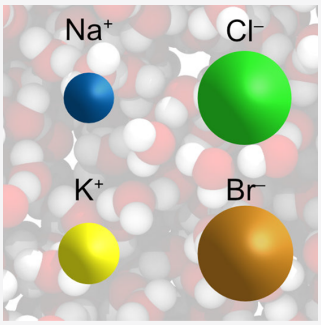

INTRODUCTION

Aqueous electrolyte solutions not only play an important role for all living organisms but also have wide electrochemical applications with many economical and environmental advantages compared to nonaqueous solvents.[1] One prominent method to investigate the properties of aqueous solutions is the use of force-field molecular dynamics simulations. The accuracy of these simulations clearly relies on the force field—the interatomic potential used to model the interactions between cations, anions, and water molecules. Besides the Coulomb interaction between charges, the simplest force fields consist of a Lennard-Jones potential to reproduce the Pauli repulsion between overlapping electron shells as well as the London dispersion. Although the latter term models induced dipole−dipole interactions and thus implicitly accounts for the atomic polarizability and ionization potential, these models are referred to as nonpolarizable due to their lack of explicit polarizability. Commonly used nonpolarizable ion force fields include those by Smith,[2,3] Dang,[4] and the Groningen Molecular Simulation (GROMOS) set[5] for the simple point charge/extended (SPC/E) water model and the Assisted Model Building with Energy Refinement (AMBER),[6] the Chemistry at Harvard Macromolecular Mechanics (CHARMM),[7] and optimized versions based on these[8] for the transferable intermolecular potential (TIP) water model family. Yet these force fields produce conflicting results for a number of important systems, including DNA[9,10] and lipid membranes,[11] and must be amended for proteins.[12]

The unreliable results have triggered a fierce and ongoing debate about the treatment of polarizability.[13−15] In particular, since the dielectric environment changes with the ion concentration, the introduction of an explicit ionic polarizability is often considered necessary. Possible implementations include inducible point dipoles, the use of Drude oscillators,[16] and, more recently, a method based on scaling the Coulomb interaction.[17,18] What these solutions have in common is the introduction of one or several parameters in addition to the existing Lennard-Jones parameters. Yet the Lennard-Jones potential already provides a large parameter space: Even using a predetermined water force field with a single Lennard-Jones interaction site, there are 10 independent interaction parameters available for a single type of monatomic salt in water (two parameters each for the cation−water, anion−water, cation−anion, cation−cation, and anion−anion interactions). Claims about the necessity of including an explicit polarizability in force fields have been made without attempting an optimization of nonpolarizable ion force fields in the complete parameter space.[15,19] In fact, it has been shown that classical nonpolarizable force fields for most monovalent

Received: June 16, 2021
Revised: June 27, 2021
Published: July 22, 2021

https://doi.org/10.1021/acs.jpcb.1c05303
J. Phys. Chem. B 2021, 125, 8581−8587

and divalent ions can be optimized to reproduce a number of bulk macroscopic thermodynamic observables[20−22] and that these force fields accurately reproduce the air−water surface affinity.[23] Nevertheless, whereas in most force fields the number of free parameters is reduced by inferring the parameters of the heterogeneous atom pairs from those of the homogeneous pairs, these so-called mixing rules must be modified for the thermodynamically optimized force fields. Moreover, the parameters of a number of ions have been selected as a reference for the optimization of the other ions,[20] equivalent to an extra-thermodynamic assumption.

A further point of dispute is the transferability of the ion force fields between water models. The most common nonpolarizable water models are the SPC/E and members of the TIP family. One of the newest offsprings of this family is the TIP4P/ε, which accurately reproduces the dielectric constant over a wide temperature range.[24] A previous attempt to construct thermodynamically consistent ion force fields for the TIP3P water model only yielded satisfactory behavior at ion concentrations used in the optimization[25] [Section S8].

Here, we introduce a classical nonpolarizable force field for K^+, Na^+, Cl^- and Br^- optimized for the SPC/E water model, the parameters of which are directly transferable to other major water models, in particular, TIP3P, TIP4P/ε, and, to a lesser degree of accuracy, TIP4P. The force field is optimized with respect to the solvation free energy of an ion pair and the activity coefficient at finite salt concentrations.[20,22] In contrast to previous work, we apply only Lorentz−Berthelot mixing rules, and by simultaneously optimizing the parameters of all four ion types, no ion parameters need to be fixed in advance. The resulting force field exhibits excellent agreement with the experimental density, ionic conductivity, and dielectric constant as a function of concentration up to 5 mol kg^{-1}. Compared with the force fields by Smith and Dang[2] used for the SPC/E water model and the CHARMM force field[26] used for the TIP family we find a significantly better agreement with experimental observables.

METHODS

Our simulation systems can be divided into two classes, namely, (1) infinite dilution systems with a single solvated ion and (2) finite concentration simulations. In the infinite dilution systems, a single ion is placed in a cubic box with a box length of L = 2.5 nm containing 509 water molecules. For systems at finite dilution we use a box length of L = 6.5 nm with different numbers of ion pairs. Each system is first energy-minimized using the steepest descent algorithm and then equilibrated for 200 ps in the *NPT* ensemble at 1 bar and 300 K. For the systems at an infinite dilution we simulate for at least 1 ns, and for the systems at a finite concentration the simulation goes for at least 20 ns.

All simulations are performed using the 2019 version of the GROMACS simulation package[27] with a 2 fs time step. The velocity rescale thermostat, including a stochastic factor,[28] is employed with a time constant of 0.5 ps. For the pressure coupling we apply the Berendsen barostat[29] with a time constant of 1 ps. A cutoff of 0.9 nm is used for the Lennard-Jones interaction, without a long-range dispersion correction.[30] The Lennard-Jones potential is shifted by its value at the cutoff. Long-range electrostatic interactions are handled using the smooth particle mesh Ewald method (SPME).[31] In all simulations we use the Lorentz−Berthelot mixing rules, given by $\sigma_{ij} = (\sigma_i + \sigma_j)/2$ and $\epsilon_{ij} = \sqrt{\epsilon_i \epsilon_j}$.

Solvation Free Energies. The solvation free energy F is obtained in the *NVT* ensemble using a two-stage thermodynamic integration method.[32] First, all Lennard-Jones interactions between the ion and other atoms are gradually turned on; second, the charge of the ion is increased from q = 0 to $\pm e$, with e being the elementary charge. The integration is performed along the reaction coordinate λ, where λ = 0 corresponds to the initial state (A), and λ = 1 corresponds to the final state (B). For the integration, the Hamiltonian is interpolated linearly, $H = (1 - \lambda)H_A + \lambda H_B$. The Lennard-Jones and charging transformations are divided into 10 steps each. Free energy differences are calculated by integrating $\langle \partial H/\partial\lambda \rangle$ from λ = 0 to λ = 1 using the alchemical-analysis toolkit.[32] For the integration of the Lennard-Jones potential, we use a soft-core potential to prevent a singularity at λ = 0,[33] with a soft-core radius α = 0.5 nm and a soft-core power p = 1.[27] The simulation time for each λ state is 1 ns. The simulated free energy F_{sim} must be corrected for the effects of the periodic boundary conditions in combination with the Ewald summation as well as for the effect of compressing an ideal gas,

$$F = F_{sim} + F_{pbc} + F_p \tag{1}$$

The first correction reads[34]

$$F_{pbc} = \frac{e^2(\varepsilon - 1)}{6\varepsilon\varepsilon_0 L}\left[\left(\frac{r}{L}\right)^2 - \frac{4\pi}{15}\left(\frac{r}{L}\right)^5\right] - \frac{e^2\xi}{8\pi\varepsilon\varepsilon_0 L} \tag{2}$$

where ξ is the Wigner constant, given by −2.837 297, ε is the dielectric constant of the water model, L is the length of the cubic box, and $r = 2^{1/6}\sigma$ is the ion's Lennard-Jones radius. The first term in eq 2 stems from the interaction of the ion with its periodic images, and the second term is derived from effects of the homogeneous background charge. For our system the correction from eq 2 equals ∼1 k_BT. The second correction equals

$$F_p = k_B T \ln(p_0/p_1) \tag{3}$$

resulting from the fact that the experimental free energy refers to a transfer of an ideal gas at pressure p_0 = 1 atm into a 1 mol/l ideal solution. Using $p_1 = k_BTn$, with n being the number density, we find $F_p = 3.2k_BT$. The experimental free energies of ion pairs at 300 K were calculated from Marcus[35] and Tissandier et al.;[36] see section S2 in the Supporting Information for details.

Ionic Activity Coefficients. The activity coefficients are obtained using Kirkwood-Buff integrals. With charge neutrality, the monovalent ion number density $n = n_+ = n_-$ can be expressed in terms of Kirkwood-Buff integrals $G^\infty_{\alpha\beta}$ as $n = (G^\infty_{+-} - G^\infty_{++})^{-1}$.[37] Therefore, the logarithmic derivative of the mean activity a with respect to n equals the following combination of Kirkwood Buff integrals

$$a_{cc} = 1 + \frac{\partial \ln \gamma}{\partial \ln n} = \frac{G^\infty_{+-} - G^\infty_{++}}{2(G^\infty_{+-} - G^\infty_{+s})} \tag{4}$$

where +, −, and s denote cation, anion, and solvent, respectively, and $\gamma = a/n$ denotes the mean molar activity coefficient of anions and cations. The Kirkwood-Buff integrals are calculated from pair correlation functions $g_{\alpha\beta}(r_1, r_2)$ according to[38]

$$G^R_{\alpha\beta}(R) = \int_0^{2R} w(r, R)[g_{\alpha\beta}(r) - 1]\, dr \tag{5}$$

https://doi.org/10.1021/acs.jpcb.1c05303
J. Phys. Chem. B 2021, 125, 8581−8587

using a geometrical weight function

$$w(r, R) = 4\pi r^2\left[1 - \frac{3r}{4R} + \frac{r^3}{16R^3}\right] \tag{6}$$

after which $G^{\infty}_{\alpha\beta}$ is obtained by a linear extrapolation of $G^{R}_{\alpha\beta}(R)$ as a function of $1/R$ to $1/R = 0$. Experimental activities are obtained from Hamer and Wu.[39]

Ionic Conductivity. According to the Einstein−Smoluchowski relation the conductivity κ of monovalent ions is given by

$$\kappa = \frac{e^2 n}{k_B T}(D^{+}_{\text{self}} + D^{-}_{\text{self}}) \tag{7}$$

where D^{+}_{self} and D^{-}_{self} denote the cationic and anionic self-diffusivities, respectively. For the self-diffusion coefficient D_{self} we use the same simulation trajectories as for the activity coefficients. The coefficients are obtained from a linear fit to the long-time mean-squared displacement (MSD) (see section S5 in the Supporting Information)

$$\langle x^2 \rangle = 6D_{\text{sim}}t + c \tag{8}$$

where the constant c accounts for short-time deviations. To account for finite size effects, we use the relation

$$D_{\text{self}} = D_{\text{sim}} + \frac{\xi k_B T}{6\pi\eta L} \tag{9}$$

where D_{sim} is the simulated self-diffusion coefficient, and η is the viscosity of the water model,[40] taken from González and Abascal.[41]

Dielectric Constant at Finite Salt Concentration. We obtain the dielectric decrement by employing a linear response formalism for salt solutions.[42] In this approach, the total electric susceptibility spectrum $\chi(\omega)$ is decomposed into three additive contributions

$$\varepsilon(\omega) = 1 + \chi(\omega) = 1 + \chi_W(\omega) + \chi_{IW}(\omega) + \chi_I(\omega) \tag{10}$$

that are related to time correlation functions between the water dipole moment, water dipole-ion current, and ion-current, respectively. The dielectric constant is then obtained from taking the limit $\omega \to 0$; see section S6.

RESULTS AND DISCUSSION

To find the optimal parameters we start by choosing Lennard-Jones parameters for the chloride ion. We then pick a set of cation parameters that lie on the solvation free energy isolines so that they reproduce the experimental solvation free energy of KCl and NaCl. For each partial parameter set (Na^+, K^+, Cl^-), we then calculate the log−log derivative a_{cc} of the activity for several concentrations and calculate the mean-squared deviation of a_{cc} from the experimental activity derivatives. For the best parameter set of chloride and the cations, we repeat the optimization for the bromide salts (KBr, NaBr) while varying the Br^- parameters and keeping the cation parameters fixed. With this strategy, the optimal parameter set only depends on the initial parameters of the chloride ion. We repeat the procedure for different choices of the Cl^- parameters. See sections S1 and S3 in the Supporting Information for additional details.

Figure 1 shows the mean-squared deviation

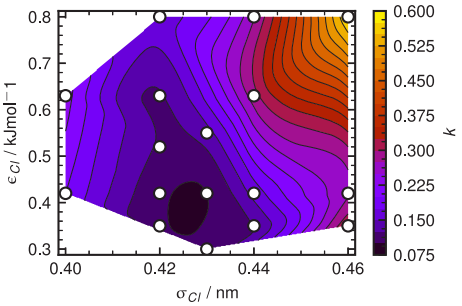

Figure 1. Mean squared difference k defined in eq 11 between the simulated a_{cc} and experimental[39] activity derivatives $a_{cc,exp}$ for the optimal parameters of the four salts, as a function of the Lennard-Jones parameters of the Cl^- ion. Circles depict the parameter combinations for which the simulations were performed, and the contour map is calculated by a cubic interpolation.

$$k = \left\langle \frac{\sum_m [a_{cc}(m) - a_{cc,exp}(m)]^2}{\sum_m} \right\rangle \tag{11}$$

from the experimental activity derivatives $a_{cc,exp}$ for all our tested initial chloride parameters. In eq 11 the $\langle \cdot \rangle$ term denotes the mean over all salts, and m indicates the molality, which is considered in the range of $0 < m$, mol/kg < 5. We find a minimum in this $\sigma-\epsilon$ landscape for $\sigma_{Cl} = 0.43$ nm and $\epsilon_{Cl} = 0.42$ kJ mol^{-1}. Our cubic interpolation suggests the minimum to be at slightly smaller σ and ϵ values. However, the effect of these small changes in the parameters on the activity coefficients can not be resolved with sufficient accuracy. Using these Lennard-Jones parameters we obtain our optimal ion parameters as shown in Table 1. Note that the third digit of

Table 1. Optimal Ion Lennard-Jones Parameters and Charges[a]

ion	σ_i (nm)	ϵ_i (kJ mol^{-1})	q (e)
K^+	0.283	0.90	+1
Na^+	0.231	0.45	+1
Cl^-	0.43	0.42	−1
Br^-	0.443	0.75	−1

[a]Lorentz-Berthelot mixing rules are used for σ_{ij} and ϵ_{ij}. The Lennard-Jones parameters of the used water models are listed in table S4 in the Supporting Information.

the σ_i parameter of sodium is important; even tiny changes in the sodium parameters have drastic effects on the activities (see Figure S3 in the Supporting Information).

Next, we test the transferability of our parameters to water models other than SPC/E. Figure 2 shows the solvation free energy for the four salts and the four water models. All free energies agree within 2% with the experimental values taken from refs 35 and 36. We find that changing the water model has a negligible effect on the solvation free energies. Symbols show the solvation free energy of the force fields from refs 2, 25, and 26.

Figure 3 shows the activity derivative a_{cc} for the four different water models by applying eq 4. For a selection of concentrations, the radial distribution functions are shown in section S4 in the Supporting Information. We also show activities for NaCl using parameters from two common force fields, by Smith and Dang[2] (pink crosses) for the SPC/E water

https://doi.org/10.1021/acs.jpcb.1c05303
J. Phys. Chem. B 2021, 125, 8581−8587

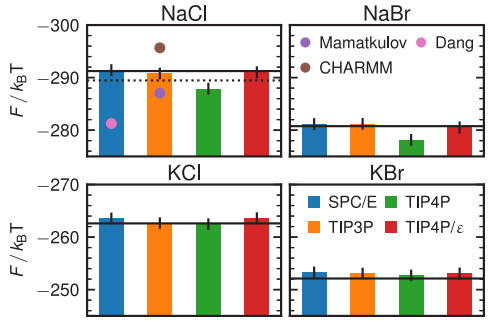

Figure 2. Salt solvation free energies for ion parameters using different water models. Experimental free energies at 300 K (solid black lines) are calculated from Marcus[35] and Tissandier et al.[36] Symbols show the solvation free energy of reported force fields.[2,25,26] The dotted black line corresponds to the solvation free energy of NaCl used in our previous work as well as in the work of Mamatkulov and Schwierz;[25] see section S2 of the Supporting Information.

model and CHARMM[26] (brown crosses) optimized for the TIP family, as well as the newer force field by Mamatkulov and Schwierz[25] optimized for TIP3P (purple crosses). As shown in Figure 3, we find good agreement between our force field results and experiments for all water models, except for the sodium salts in the TIP4P water model. This shows that the same ion force fields can be used in combination with all major nonpolarizable water models, in contrast to previous suggestions.[25] In general, we find that the agreement between all water models is better for the potassium salts compared to the sodium salts. Our optimization also shows that the potassium salts are more robust with regard to a variation of the parameters (Figure S3 of the Supporting Information).

Finally, we test the ion parameters against a number of experimental observables that we did not optimize for. In Figure 4, we show the mass density ρ, the conductivity κ (eqs 7 and 8), the dielectric decrement $\Delta\varepsilon$ (eq 10), and the water self-diffusion constant D (eqs 8 and 9). The density increment in Figure 4a shows excellent agreement with the experimental data. The higher density of the bromide salts is due to the much higher molar mass of bromide (m_{Br} = 79.90 u) compared to chloride (m_{Cl} = 35.45 u). The conductivity in Figure 4b shows a quantitative agreement with the experimental data for all salts up to at least 2 mol/kg. A selection of MSDs are shown in section S5 in the Supporting Information. We find that the

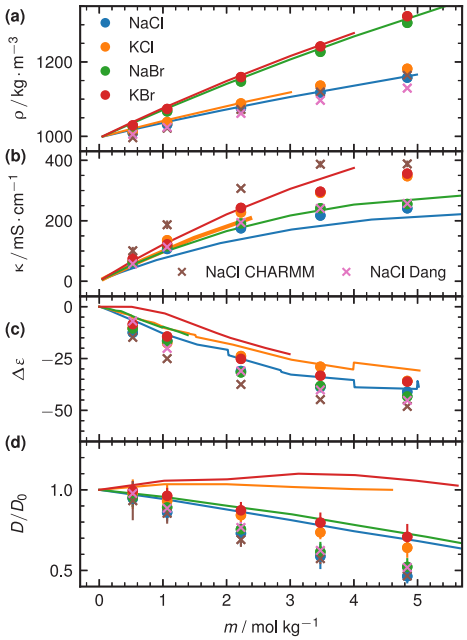

Figure 4. (a) Simulated mass density ρ for the four salts using the optimized force field (●) and literature force fields[2,26] (×) together with the experimental densities[43,44] (solid lines) as a function of the salt concentration. (b) Ionic conductivities κ together with the experimental values (solid lines).[43,45] (c) Dielectric decrement $\Delta\varepsilon$ together with the experimental values (solid lines).[46−53] (d) Water diffusion constant normalized by its value for pure water together with the experimental values (solid lines).[54] The SPC/E water model is used in all panels. Results from other water models are shown in Figure S8.

sodium salts have a lower conductivity when compared to the potassium salts. Because of the small size of sodium, it exhibits a strong hydrogen bonding to water molecules, reducing its diffusion constant compared to potassium. This effect is faithfully reproduced by our new force field. The dielectric decrement $\Delta\varepsilon$, displayed in Figure 4c, is obtained by subtracting the bulk water dielectric constant for SPC/E, $\varepsilon_{SPC/E}$ = 72.0, from the dielectric constant calculated using eq 10. The experimental values are taken from refs 46−53 and have been averaged for each salt type. Both the trend and the

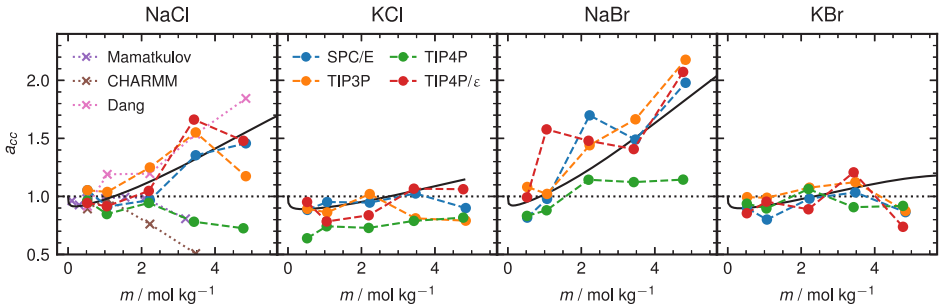

Figure 3. Activity derivative according to eq 4 of NaCl, KCl, NaBr, KBr as a function of the salt concentration. Different colors depict different water models. The cross symbols denote results from the force fields by Smith and Dang[2] (SPC/E, pink), CHARMM[26] (TIP3P, brown), and reproduced from Mamatkulov and Schwierz[25] (TIP3P, purple). Solid black lines depict the experimental activity derivatives.[39] Errors are between 0.1 and 0.3 (estimated using a block averaging with five blocks; see Figure S4 for individual error bars).

https://doi.org/10.1021/acs.jpcb.1c05303
J. Phys. Chem. B 2021, 125, 8581−8587

amplitude of $\Delta\varepsilon$ are accurately captured by our new force field. The water diffusion coefficient, calculated from eqs 8 and 9, is shown in Figure 4d. Again, the order of the ions is well-reproduced. However, the simulated water diffusivity for the potassium salts fails to capture the experimental trend as a function of the salt concentration. This issue has been noticed for rigid nonpolarizable water models before.[55] To compare with other NaCl force fields, we show the results for Smith and Dang[2] and CHARMM[26] as pink and brown symbols in Figure 4a–d, respectively. Overall, our new force field agrees better with the experimental NaCl data, but note that the density using the CHARMM[26] parameters coincides with our results. For the other water models, the observables show a very similar behavior (see Figure S8 of the Supporting Information), confirming the transferability of the ion parameters between the water models.

CONCLUSION

We have optimized a nonpolarizable force field for aqueous solutions of NaCl, KCl, NaBr, and KBr up to concentrations of 5 mol/kg. In contrast to previous work, all Lennard-Jones parameters are determined rigorously by simultaneously optimizing four ion pairs with respect to the experimental solvation free energy and the activity, in combination with standard mixing rules. This procedure eliminates the necessity to select a reference ion, which turns out to be crucial for the performance of the resulting force field. The force field is fully transferable between the rigid water models SPC/E, TIP3P, and TIP4P/ε. In TIP4P, the activity of the sodium salts is poorly reproduced, which is likely to be related to the inferior dielectric properties of TIP4P.[24] The previously used modified mixing rules for heterogeneous atom pairs,[20] although perfectly compatible with the current optimization strategy, are unnecessary for these ions. Our new force field reproduces the dependence of the density, the conductivity, and the dielectric decrement on the salt concentration over the entire concentration range, but not the water self-diffusion constant. The successful optimization shows that an explicit polarizability is unnecessary despite the strong variation of the dielectric constant with the salt concentration. Instead, standard Coulomb and Lennard-Jones interactions are sufficient to accurately capture the macroscopic thermodynamics of aqueous ionic solutions, as well as the conductivity and the dielectric constant. Note that more complex water and ion models might be necessary to capture other kinetic properties, such as the water self-diffusion coefficient.[55] In conclusion, the newly optimized force field ensures that the electrolyte thermodynamics are accurately reproduced in simulations with the most widely used water models without introducing a more complex interaction potential.

ASSOCIATED CONTENT

Supporting Information

The Supporting Information is available free of charge at https://pubs.acs.org/doi/10.1021/acs.jpcb.1c05303.

Details of the optimization procedure, calculation of the diffusivity and the dielectric decrement, observables for different water models, and discussion of the comparison to other force fields (PDF)

AUTHOR INFORMATION

Corresponding Author

Douwe Jan Bonthuis − *Institute of Theoretical and Computational Physics, Graz University of Technology, 8010 Graz, Austria;* orcid.org/0000-0002-1252-7745; Email: bonthuis@tugraz.at

Authors

Philip Loche − *Fachbereich Physik, Freie Universität Berlin, 14195 Berlin, Germany;* orcid.org/0000-0002-9112-0010

Patrick Steinbrunner − *Fachbereich Physik, Freie Universität Berlin, 14195 Berlin, Germany*

Sean Friedowitz − *Department of Materials Science and Engineering, Stanford University, Stanford 94305 California, United States*

Roland R. Netz − *Fachbereich Physik, Freie Universität Berlin, 14195 Berlin, Germany;* orcid.org/0000-0003-0147-0162

Complete contact information is available at: https://pubs.acs.org/10.1021/acs.jpcb.1c05303

Notes

The authors declare no competing financial interest.

Data Availability Original simulation and analysis files are available at http://dx.doi.org/10.17169/refubium-30888.

ACKNOWLEDGMENTS

Funding by the Deutsche Forschungsgemeinschaft via Grant No. SFB 1349, Project-ID 387284271 is gratefully acknowledged. S.F. acknowledges funding from the Stanford GRIP fellowship for his contributions.

REFERENCES

(1) Tomiyasu, H.; Shikata, H.; Takao, K.; Asanuma, N.; Taruta, S.; Park, Y.-Y. An aqueous electrolyte of the widest potential window and its superior capability for capacitors. *Sci. Rep.* **2017**, *7*, 1−12.

(2) Smith, D. E.; Dang, L. X. Computer simulations of NaCl association in polarizable water. *J. Chem. Phys.* **1994**, *100*, 3757−3766.

(3) Weerasinghe, S.; Smith, P. E. A Kirkwood−Buff derived force field for sodium chloride in water. *J. Chem. Phys.* **2003**, *119*, 11342−11349.

(4) Dang, L. X. Mechanism and Thermodynamics of Ion Selectivity in Aqueous Solutions of 18-Crown-6 Ether: A Molecular Dynamics Study. *J. Am. Chem. Soc.* **1995**, *117*, 6954−6960.

(5) Oostenbrink, C.; Villa, A.; Mark, A. E.; Van Gunsteren, W. F. A Biomolecular Force Field Based on the Free Enthalpy of Hydration and Solvation: The GROMOS Force-Field Parameter Sets 53A5 and 53A6. *J. Comput. Chem.* **2004**, *25*, 1656−1676.

(6) Wang, J.; Wolf, R. M.; Caldwell, J. W.; Kollman, P. A.; Case, D. A. Development and testing of a general amber force field. *J. Comput. Chem.* **2004**, *25*, 1157−1174.

(7) Vanommeslaeghe, K.; Hatcher, E.; Acharya, C.; Kundu, S.; Zhong, S.; Shim, J.; Darian, E.; Guvench, O.; Lopes, P.; Vorobyov, I.; et al. CHARMM general force field: A force field for drug-like molecules compatible with the CHARMM all-atom additive biological force fields. *J. Comput. Chem.* **2010**, *31*, 671−690.

(8) Joung, I. S.; Cheatham, T. E. Determination of Alkali and Halide Monovalent Ion Parameters for Use in Explicitly Solvated Biomolecular Simulations. *J. Phys. Chem. B* **2008**, *112*, 9020−9041.

(9) Cheatham, T. E., III; Kollman, P. A. Molecular Dynamics Simulations Highlight the Structural Differences among DNA:DNA, RNA:RNA, and DNA:RNA Hybrid Duplexes. *J. Am. Chem. Soc.* **1997**, *119*, 4805−4825.

https://doi.org/10.1021/acs.jpcb.1c05303
J. Phys. Chem. B 2021, 125, 8581−8587

(10) Yoo, J.; Aksimentiev, A. Improved Parametrization of Li^+, Na^+, K^+, and Mg^{2+} Ions for All-Atom Molecular Dynamics Simulations of Nucleic Acid Systems. *J. Phys. Chem. Lett.* **2012**, *3*, 45−50.
(11) Valley, C. C.; Perlmutter, J. D.; Braun, A. R.; Sachs, J. N. NaCl Interactions with Phosphatidylcholine Bilayers do Not Alter Membrane Structure but Induce Long-Range Ordering of Ions and Water. *J. Membr. Biol.* **2011**, *244*, 35−42.
(12) Hess, B.; Van der Vegt, N. F. A. Cation specific binding with protein surface charges. *Proc. Natl. Acad. Sci. U. S. A.* **2009**, *106*, 13296−13300.
(13) Perera, L.; Berkowitz, M. L. Many-body effects in molecular dynamics simulations of Na+(H2O)n and Cl-(H2O)n clusters. *J. Chem. Phys.* **1991**, *95*, 1954−1963.
(14) Jungwirth, P.; Tobias, D. J. Specific Ion Effects at the Air/Water Interface. *Chem. Rev.* **2006**, *106*, 1259−1281.
(15) Jing, Z.; Liu, C.; Cheng, S. Y.; Qi, R.; Walker, B. D.; Piquemal, J.-P.; Ren, P. Polarizable Force Fields for Biomolecular Simulations: Recent Advances and Applications. *Annu. Rev. Biophys.* **2019**, *48*, 371−394.
(16) Lamoureux, G.; MacKerell, A. D.; Roux, B. A simple polarizable model of water based on classical Drude oscillators. *J. Chem. Phys.* **2003**, *119*, 5185−5197.
(17) Kohagen, M.; Mason, P. E.; Jungwirth, P. Accounting for Electronic Polarization Effects in Aqueous Sodium Chloride via Molecular Dynamics Aided by Neutron Scattering. *J. Phys. Chem. B* **2016**, *120*, 1454−1460.
(18) Zeron, I. M.; Abascal, J. L. F.; Vega, C. A force field of Li+, Na+, K+, Mg2+, Ca2+, C-, and SO42- in aqueous solution based on the TIP4P/2005 water model and scaled charges for the ions. *J. Chem. Phys.* **2019**, *151*, 134504.
(19) Kirby, B. J.; Jungwirth, P. Charge Scaling Manifesto: A Way of Reconciling the Inherently Macroscopic and Microscopic Natures of Molecular Simulations. *J. Phys. Chem. Lett.* **2019**, *10*, 7531−7536.
(20) Fyta, M.; Netz, R. R. Ionic force field optimization based on single-ion and ion-pair solvation properties: Going beyond standard mixing rules. *J. Chem. Phys.* **2012**, *136*, 124103.
(21) Mamatkulov, S.; Fyta, M.; Netz, R. R. Force fields for divalent cations based on single-ion and ion-pair properties. *J. Chem. Phys.* **2013**, *138*, 024505.
(22) Bonthuis, D. J.; Mamatkulov, S. I.; Netz, R. R. Optimization of classical nonpolarizable force fields for OH- and H3O+. *J. Chem. Phys.* **2016**, *144*, 104503.
(23) Mamatkulov, S. I.; Allolio, C.; Netz, R. R.; Bonthuis, D. J. Orientation-Induced Adsorption of Hydrated Protons at the Air−Water Interface. *Angew. Chem., Int. Ed.* **2017**, *56*, 15846−15851.
(24) Fuentes-Azcatl, R.; Alejandre, J. Non-Polarizable Force Field of Water Based on the Dielectric Constant: TIP4P/epsilon. *J. Phys. Chem. B* **2014**, *118*, 1263−1272.
(25) Mamatkulov, S.; Schwierz, N. Force fields for monovalent and divalent metal cations in TIP3P water based on thermodynamic and kinetic properties. *J. Chem. Phys.* **2018**, *148*, 074504.
(26) Venable, R. M.; Luo, Y.; Gawrisch, K.; Roux, B.; Pastor, R. W. Simulations of Anionic Lipid Membranes: Development of Interaction-Specific Ion Parameters and Validation Using NMR Data. *J. Phys. Chem. B* **2013**, *117*, 10183−10192.
(27) Abraham, M. J.; Murtola, T.; Schulz, R.; Páll, S.; Smith, J. C.; Hess, B.; Lindahl, E. GROMACS: High performance molecular simulations through multi-level parallelism from laptops to supercomputers. *SoftwareX* **2015**, *1−2*, 19−25.
(28) Bussi, G.; Donadio, D.; Parrinello, M. Canonical sampling through velocity rescaling. *J. Chem. Phys.* **2007**, *126*, 014101.
(29) Berendsen, H. J. C.; Postma, J. P. M.; van Gunsteren, W. F.; DiNola, A.; Haak, J. R. Molecular dynamics with coupling to an external bath. *J. Chem. Phys.* **1984**, *81*, 3684−3690.
(30) Berendsen, H. J. C.; Grigera, J. R.; Straatsma, T. P. The missing term in effective pair potentials. *J. Phys. Chem.* **1987**, *91*, 6269−6271.
(31) Essmann, U.; Perera, L.; Berkowitz, M. L.; Darden, T.; Lee, H.; Pedersen, L. G. A smooth particle mesh Ewald method. *J. Chem. Phys.* **1995**, *103*, 8577−8593.
(32) Klimovich, P. V.; Shirts, M. R.; Mobley, D. L. Guidelines for the analysis of free energy calculations. *J. Comput.-Aided Mol. Des.* **2015**, *29*, 397−411.
(33) Beutler, T. C.; Mark, A. E.; van Schaik, R. C.; Gerber, P. R.; van Gunsteren, W. F. Avoiding singularities and numerical instabilities in free energy calculations based on molecular simulations. *Chem. Phys. Lett.* **1994**, *222*, 529−539.
(34) Hünenberger, P. H.; McCammon, J. A. Ewald artifacts in computer simulations of ionic solvation and ion−ion interaction: A continuum electrostatics study. *J. Chem. Phys.* **1999**, *110*, 1856−1872.
(35) Marcus, Y. *Ion Properties;* Taylor & Francis, 1997.
(36) Tissandier, M. D.; Cowen, K. A.; Feng, W. Y.; Gundlach, E.; Cohen, M. H.; Earhart, A. D.; Coe, J. V.; Tuttle, T. The Proton's Absolute Aqueous Enthalpy and Gibbs Free Energy of Solvation from Cluster-Ion Solvation Data. *J. Phys. Chem. A* **1998**, *102*, 7787−7794.
(37) Kusalik, P. G.; Patey, G. N. The thermodynamic properties of electrolyte solutions: Some formal results. *J. Chem. Phys.* **1987**, *86*, 5110−5116.
(38) Krüger, P.; Schnell, S. K.; Bedeaux, D.; Kjelstrup, S.; Vlugt, T. J. H.; Simon, J.-M. Kirkwood−Buff Integrals for Finite Volumes. *J. Phys. Chem. Lett.* **2013**, *4*, 235−238.
(39) Hamer, W. J.; Wu, Y. Osmotic Coefficients and Mean Activity Coefficients of Uni-univalent Electrolytes in Water at 25C. *J. Phys. Chem. Ref. Data* **1972**, *1*, 1047−1100.
(40) Yeh, I.-C.; Hummer, G. System-Size Dependence of Diffusion Coefficients and Viscosities from Molecular Dynamics Simulations with Periodic Boundary Conditions. *J. Phys. Chem. B* **2004**, *108*, 15873−15879.
(41) González, M. A.; Abascal, J. L. F. The shear viscosity of rigid water models. *J. Chem. Phys.* **2010**, *132*, 096101.
(42) Rinne, K. F.; Gekle, S.; Netz, R. R. Dissecting ion-specific dielectric spectra of sodium-halide solutions into solvation water and ionic contributions. *J. Chem. Phys.* **2014**, *141*, 214502.
(43) Isono, T. Density, viscosity, and electrolytic conductivity of concentrated aqueous electrolyte solutions at several temperatures. Alkaline-earth chlorides, lanthanum chloride, sodium chloride, sodium nitrate, sodium bromide, potassium nitrate, potassium bromide, and cadmium nitrate. *J. Chem. Eng. Data* **1984**, *29*, 45−52.
(44) Gates, J. A.; Wood, R. H. Densities of aqueous solutions of sodium chloride, magnesium chloride, potassium chloride, sodium bromide, lithium chloride, and calcium chloride from 0.05 to 5.0 mol kg-1 and 0.1013 to 40 MPa at 298.15 K. *J. Chem. Eng. Data* **1985**, *30*, 44−49.
(45) Weast, R. C. *CRC Handbook of Chemistry and Physics,* 70th ed.;CRC Press, 1989.
(46) Hasted, J. B.; Ritson, D. M.; Collie, C. H. Dielectric Properties of Aqueous Ionic Solutions. Parts I and II. *J. Chem. Phys.* **1948**, *16*, 1−21.
(47) Haggis, G. H.; Hasted, J. B.; Buchanan, T. J. The Dielectric Properties of Water in Solutions. *J. Chem. Phys.* **1952**, *20*, 1452−1465.
(48) Barthel, J. *Electrolyte Data Collection: Dielectric Properties of Water and Aqueous Electrolyte Solutions (Chemistry Data Series);* Dechema, 1996.
(49) Chen, T.; Hefter, G.; Buchner, R. Dielectric Spectroscopy of Aqueous Solutions of KCl and CsCl. *J. Phys. Chem. A* **2003**, *107*, 4025−4031.
(50) Wachter, W.; Kunz, W.; Buchner, R.; Hefter, G. Is There an Anionic Hofmeister Effect on Water Dynamics? Dielectric Spectroscopy of Aqueous Solutions of NaBr, NaI, NaNO3, NaClO4, and NaSCN. *J. Phys. Chem. A* **2005**, *109*, 8675−8683.
(51) Abascal, J. L. F.; Vega, C. A general purpose model for the condensed phases of water: TIP4P/2005. *J. Chem. Phys.* **2005**, *123*, 234505.
(52) Levy, A.; Andelman, D.; Orland, H. Dielectric Constant of Ionic Solutions: A Field-Theory Approach. *Phys. Rev. Lett.* **2012**, *108*, 227801.
(53) Shcherbakov, V. V.; Artemkina, Y. M.; Korotkova, E. N. Dielectric properties and high-frequency conductivity of the sodium chloride-water system. *Russ. J. Inorg. Chem.* **2014**, *59*, 922−926.

https://doi.org/10.1021/acs.jpcb.1c05303
J. Phys. Chem. B 2021, 125, 8581−8587

(54) Müller, K. J.; Hertz, H. G. A Parameter as an Indicator for Water-Water Association in Solutions of Strong Electrolytes. *J. Phys. Chem.* **1996**, *100*, 1256−1265.
(55) Yao, Y.; Berkowitz, M. L.; Kanai, Y. Communication: Modeling of concentration dependent water diffusivity in ionic solutions: Role of intermolecular charge transfer. *J. Chem. Phys.* **2015**, *143*, 241101.

https://doi.org/10.1021/acs.jpcb.1c05303
J. Phys. Chem. B 2021, 125, 8581−8587

4

ELECTROSTATICS OF PLANAR NANO SYSTEMS

Water in nanometer confinement exhibits properties that are drastically different from bulk. This is particularly true for the dielectric constant, which becomes anisotropic in confinement. Recent experiments in the Geim group [24] demonstrated a significant decrease of the perpendicular dielectric constant for water confined between graphene and boron-nitride sheets at nanometer separations, and by that confirmed earlier simulation predictions [52] for a single surface type. But how dielectric properties in confinement translate to electrostatic interactions and how surface properties (soft/hard, non-polar/polar) influence the dielectric response of confined water has remained unclear.

In this chapter, a multi-scale approach to address these questions is employed. By all-atom MD simulations, four different surfaces that span the entire range from soft to hard and from polar to non-polar are studied; namely graphene sheets, decanol self-assembled monolayers, phospholipid (DMPC) and glycolipid (DGDG) bilayers. The dielectric profiles in parallel and perpendicular directions differ significantly, but all decay to the bulk value within 1–2 nm from the surface constituting a universal property of nano-confined water. As shown in chapter 6 for calculating ion-ion interactions agreeing on the linear level with simulations the exact dielectric properties of the system are fundamental. The permittivities derived here are used together with the solution of the tensorial Poisson equation in planar geometries, derived by Ayaz [53]. The analytic solution reveals that ion-ion interactions are enhanced significantly in confinement. The results of this chapter impact the description of all electrostatics in aqueous nano-confinement and are thus relevant for the growing field of wet nanoscience.

DATA AVAILABILITY

The data that support the findings of this chapter are included in the SI of the publication. The simulations are carried out with the 2016 version of the GROMACS simulation package and all analyses are performed with MAICoS. Original simulation and analysis files are available at

http://dx.doi.org/10.17169/refubium-27381.

THE JOURNAL OF PHYSICAL CHEMISTRY B

pubs.acs.org/JPCB Article

Universal and Nonuniversal Aspects of Electrostatics in Aqueous Nanoconfinement

Philip Loche, Cihan Ayaz, Amanuel Wolde-Kidan, Alexander Schlaich, and Roland R. Netz*

Cite This: J. Phys. Chem. B 2020, 124, 4365−4371 Read Online

ACCESS | Metrics & More | Article Recommendations | Supporting Information

ABSTRACT: Dielectric water properties, which significantly change in confinement, determine electrostatic interactions and thereby influence all molecular forces and chemical reactions. We present comparative simulations of water between graphene sheets, decanol monolayers, and phospholipid and glycolipid bilayers. Generally, dielectric profiles strongly differ in perpendicular and parallel surface directions and for large surface separation decay to the bulk value 1−2 nm away from the surface. Polar surface groups enhance the local interfacial dielectric response and for phospholipid bilayers induce a giant parallel contribution. A mapping on a box model with asymptotically determined effective water layer widths demonstrates that the perpendicular effective dielectric constant for all systems decreases for confinement below a nanometer, while the parallel one stays rather constant. The confinement-dependent perpendicular effective dielectric constant for graphene is in agreement with experimental data only if the effective water layer width is suitably adjusted. The interactions between two charges at small separation depend on the product of parallel and perpendicular effective water dielectric components; for large separation the interactions depend on the confining medium. For metallic confining media the interactions at large separation decay exponentially with a decay length that depends on the ratio of the effective parallel and perpendicular water dielectric components.

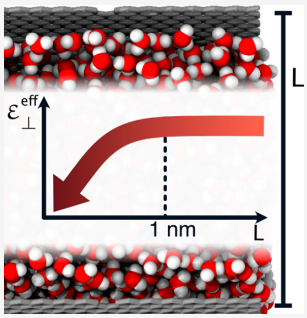

INTRODUCTION

Biologically and technologically relevant surfaces in contact with water exhibit a wide range of elastic behavior from soft (e.g., lipid bilayers) to hard (e.g., minerals and metal oxide surfaces) and a wide range of polarities from surfaces that are completely wetted by water to surfaces that are hydrophobic, such as graphene. In the past decades nanometer cavities filled with water moved into the focus because of novel assembly methods and promising applications.[1−10] It is generally acknowledged that changed water properties in nanopores and nanoslits significantly modify surface interactions, ionic adsorption, molecular transport, and chemical reaction equilibria,[11−21] but the precise mechanisms behind this relation are not clear. One fundamental property of water is its dielectric constant, which directly affects electrostatics and thereby influences, among other phenomena, surface interactions and electrokinetics.[22−24] Clearly, all models and theories that involve charges need as input precise characterization of the electrostatic interactions, which in turn depend on the dielectric properties. By simulations and experiments, it was shown that for planar confined systems, the dielectric properties of water become anisotropic.[24−31] In particular, it was recently demonstrated that the effective perpendicular dielectric component decreases significantly in strong confinement.[29,30] This would suggest that ion−ion interactions in water change dramatically in nanoconfinement and that all static and kinetic electrolyte properties are modified as well. But how to derive meaningful effective dielectric quantities from simulations and experiments, how to calculate ion−ion interactions in confinement in the presence of tensorial dielectric constants, and the influence of the surface type on the water dielectric properties in confinement are far from settled. A fundamental problem that shows up in this context is that the effective tensorial dielectric constants of nanoconfined water depend on details of the model used for their definition. In particular, for a box model, where the effective dielectric constants are assumed to be constant in a slab of finite width, the effective dielectric constants depend sensitively on the chosen slab thickness, as has been demonstrated in experiments[30] and simulations.[29,32] This problem can in fact be elegantly solved in molecular simulations, since the local dielectric constants in the water slab center can be directly accessed in a model-free fashion and used to check the validity of the model employed in the definition of the effective dielectric constants.

Received: March 5, 2020
Revised: April 27, 2020
Published: May 4, 2020

https://dx.doi.org/10.1021/acs.jpcb.0c01967
J. Phys. Chem. B 2020, 124, 4365−4371

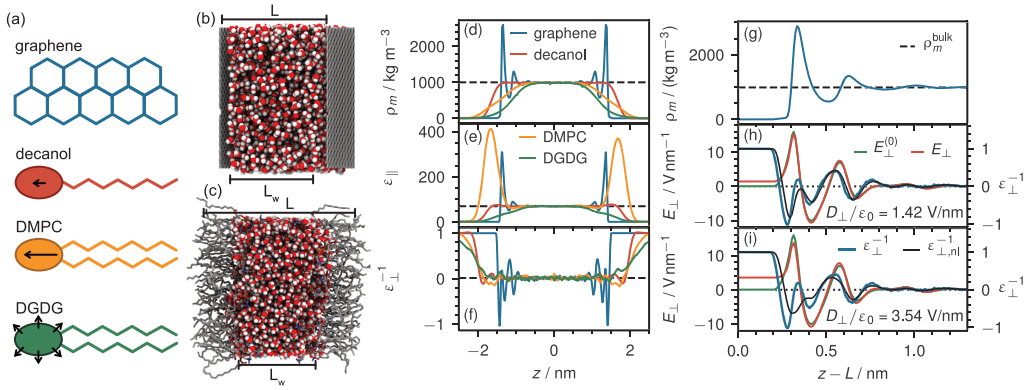

Figure 1. (a) Schematics of the constituents of the different surfaces. (b) Simulation snapshots of the graphene (water slab thickness L_w = 3.0 nm) and (c) the DMPC lipid bilayer system (L_w = 2.9 nm). (d) Water mass density profiles $\rho_m(z)$, (e) parallel dielectric profiles $\varepsilon_\parallel(z)$, and (f) inverse perpendicular dielectric profiles $\varepsilon_\perp^{-1}(z)$ for graphene (L_w = 3.0 nm), decanol (L_w = 3.3 nm), DMPC (L_w = 2.9 nm), and DGDG systems (L_w = 2.3 nm). The horizontal dashed lines denote the SPC/E water bulk values ρ_m^{bulk} = 987 kg/m^3, ε_{bulk} = 70. (g) Interfacial water mass density profile for the graphene system (same as in (d)). (h) Electric field profile $E_\perp(z)$ in the presence of an external displacement field $D_\perp/\varepsilon_0$ = 1.42 V/nm (red line) compared with the electric field profile $E_\perp^{(0)}(z)$ for $D_\perp$ = 0 (green line). The dielectric linear-response profile $\varepsilon_\perp^{-1}$ (blue line) from polarization fluctuations is compared to the dielectric profile extracted from the induced polarizations via $\varepsilon_{\perp,nl}^{-1} = \varepsilon_0(E_\perp - E_\perp^{(0)})/D_\perp$ (black line). (i) Results for $D_\perp/\varepsilon_0$ = 3.54 V/nm.

RESULTS AND DISCUSSION

Here we investigate the dielectric properties of water confined between planar surfaces. To span the entire range from soft to hard and from polar to nonpolar surfaces, we consider decanol (using our previously obtained results[29]) as well as graphene, phospholipid dipalmitoylphosphatidylcholine (DMPC) and glycolipid digalactosyldiacylglycerol (DGDG) bilayers; see Figure 1a. Water between graphene layers has unique frictional and chemical properties and is widely studied experimentally;[4,6,9] decanol layers are prototypical self-assembled monolayers (SAMs).[33,34] Phospholipid bilayers are strongly polar due to their zwitterionic nature.[35] Contrarily, DGDG head groups contain multiple OH groups, which gives rise to a characteristic swelling behavior in water.[36] We find that polar surface groups significantly contribute to the dielectric response and for DMPC bilayers, but not the other polar surfaces, give rise to a giant local parallel response. From the simulated tensorial dielectric profiles we extract a tensorial dielectric slab model in terms of effective dielectric widths and effective perpendicular and parallel dielectric constants $\varepsilon_\perp^{eff}$ and $\varepsilon_\parallel^{eff}$. While the effective dielectric widths differ considerably between different surface types, we find universal behavior for $\varepsilon_\perp^{eff}$ and $\varepsilon_\parallel^{eff}$: $\varepsilon_\parallel^{eff}$ stays rather constant at its bulk value down to subnanometer confinement, while $\varepsilon_\perp^{eff}$ decreases substantially below 1 nm. In fact, our derived $\varepsilon_\perp^{eff}$ values for water between graphene agree with recent experimental results if the effective width is suitably chosen.[30] Finally, our solution of the tensorial Poisson equation in planar geometry demonstrates that the electrostatic interaction between two charges with small separation depends on the product of $\varepsilon_\perp^{eff}$ and $\varepsilon_\parallel^{eff}$. Since $\varepsilon_\perp^{eff}$ decreases drastically for strong confinements while $\varepsilon_\parallel^{eff}$ stays approximately constant, ion interactions in strong confinement are significantly enhanced compared to bulk. For large separation, ion interactions depend on the outside medium. In particular, if the outside medium is a metal, electrostatic interactions are exponentially damped with a decay constant that depends on the ratio of $\varepsilon_\parallel^{eff}$ and $\varepsilon_\perp^{eff}$. These results are fundamental for the description of all electrostatics in aqueous nanoconfinement.

We simulate SPC/E water between four different planar surfaces at fixed L; see Figure 1a for schematics of the surface constituents. For graphene L denotes the distance between the atomic centers in the graphene sheets. For the other systems (decanol, DMPC, DGDG) L denotes the periodic simulation box length. Figure 1b and Figure 1c show snapshots of the graphene and DMPC systems, respectively. The water number N_w is fixed at a value to keep the water chemical potential or the pressure fixed. We define the water layer thickness L_w using the bulk molecular water volume v_w = 0.0304 nm^3 as $L_w = N_w v_w/A$, where A is the lateral simulation box area. By this, L_w is equivalent to the separation between the Gibbs dividing surfaces at large surface separation (see Supporting Information sections S1 and S2 for model and simulation details).

In Figure 1d we show the water mass density profiles $\rho_m(z)$. For graphene, water exhibits pronounced layering, as expected on rigid flat surfaces. For the other softer surfaces, density profiles are smooth and change monotonically. Figure 1e and Figure 1f show the parallel $\varepsilon_\parallel(z)$ and the inverse perpendicular dielectric profiles $\varepsilon_\perp^{-1}(z)$ that are obtained from polarization density fluctuations at zero external field and fully account for nonlocal response effects (see Supporting Information section S3 for details). The dielectric profiles include water and surface polarizations, and the pure water contributions are shown in the Supporting Information section S3. The parallel dielectric profiles $\varepsilon_\parallel(z)$ in Figure 1e closely follow the mass density profiles for all surfaces except DMPC; for DMPC lipids we find a giant parallel response of $\varepsilon_\parallel \approx 400$ at the interface, in agreement with earlier results,[25] which is due to the freely orientable zwitterionic head-group charges. The inverse perpendicular profiles $\varepsilon_\perp^{-1}(z)$ in Figure 1f look very different from $\rho_m(z)$ and $\varepsilon_\parallel(z)$ and cross zero at least once. In fact, the divergencies of $\varepsilon_\perp(z)$ are unproblematic and reflect dielectric overscreening effects.[24,37]

https://dx.doi.org/10.1021/acs.jpcb.0c01967
J. Phys. Chem. B 2020, 124, 4365−4371

The Journal of Physical Chemistry B pubs.acs.org/JPCB Article

How reliable are the linear dielectric response profiles shown in Figure 1e and Figure 1f? In Figure 1h and Figure 1i we show results for graphene in the presence of external perpendicular displacement fields of $D_\perp/\varepsilon_0$ = 1.42 V/nm and 3.54 V/nm, respectively. Note that these fields are, due to periodic image effects, significantly larger than the nominally applied fields of $D'_\perp/\varepsilon_0$ = 1.0 V/nm and 2.5 V/nm.[25,38] Green lines show the electric field $E_\perp^{(0)}(z)$ for $D_\perp$ = 0 and red lines show $E_\perp(z)$ for finite $D_\perp$, both obtained from integrating over the charge density profile according to $E_\perp(z) = \int_{-\infty}^{z}\rho(z')\,dz'/\varepsilon_0$. Blue lines show the linear response $\varepsilon_\perp^{-1}(z)$ from Figure 1f obtained from polarization fluctuations at zero external field, while black lines show the nonlinear dielectric profile estimated from the field-induced polarization according to $\varepsilon_{\perp,\mathrm{nl}}^{-1} = \varepsilon_0(E_\perp - E_\perp^{(0)})/D_\perp$. Surprisingly, even for a relatively high applied field of $D_\perp/\varepsilon_0$ = 1.42 V/nm, which corresponds to the field created by a planar surface with charge density σ = 0.1 e nm^{-2}, the linear dielectric profile describes the actual polarization response in Figure 1h very well, meaning that our formulation of the inhomogeneous linear dielectric response is highly accurate. For $D_\perp/\varepsilon_0$ = 3.54 V/nm in Figure 1i deviations between the black and blue lines are clearly noticeable, which indicates the onset of the breakdown of linear response theory[24,37] (results including higher field strengths are shown for the entire simulation box width in the Supporting Information section S3). Comparing the profiles for $\varepsilon_\perp^{-1}(z)$ and $E_0(z)$ in Figure 1h and Figure 1i with $\rho_m(z)$ in Figure 1g, we find all profiles to be different from each other and even the positions of the extrema not to match; we conclude that perpendicular dielectric profiles are not related to polarization and density profiles in an obvious manner.

In order to investigate the consequences of our findings for electrostatic interactions, we need to replace the complex profiles $\varepsilon_\parallel(z)$ and $\varepsilon_\perp^{-1}(z)$ by analytically manageable expressions, for which we choose step profiles[29]

$$\varepsilon_\alpha^*(z) = \begin{cases} \varepsilon_\alpha^{\mathrm{eff}} & \text{if } |z| \le L_\alpha^{\mathrm{eff}}/2 \\ 1 & \text{if } |z| > L_\alpha^{\mathrm{eff}}/2 \end{cases} \tag{1}$$

The parameters, i.e., the effective dielectric constants $\varepsilon_\alpha^{\mathrm{eff}}$ and the effective dielectric widths L_α^{eff} for parallel and perpendicular directions $\alpha = \perp, \parallel$, are obtained using dielectric effective medium theory in the following manner: For the perpendicular component we demand that the integral over $E_\perp(z)$ induced by a constant $D_\perp$ field is exactly reproduced by the box profile, which leads to[29]

$$\frac{1}{\varepsilon_\perp^{\mathrm{eff}}} = 1 + \frac{\int_{-L/2}^{L/2}\varepsilon_\perp^{-1}(z)\,dz - L}{L_\perp^{\mathrm{eff}}} \tag{2}$$

For the parallel component we demand that the integral over $D_\parallel(z)$ induced by a constant $E_\parallel$ field is reproduced by the box profile, which leads to

$$\varepsilon_\parallel^{\mathrm{eff}} = 1 + \frac{\int_{-L/2}^{L/2}\varepsilon_\parallel(z)\,dz - L}{L_\parallel^{\mathrm{eff}}} \tag{3}$$

See Supporting Information section S3 for detailed derivations. Obviously, the four parameters $\varepsilon_\alpha^{\mathrm{eff}}$ and L_α^{eff} of the effective model cannot be uniquely derived from the simulated dielectric profiles using the two eqs 2 and 3. However, we expect that for large water slab thickness L_w the effective dielectric constants $\varepsilon_\alpha^{\mathrm{eff}}$ approach the bulk value $\varepsilon_{\mathrm{bulk}}$; this asymptotic property can be used to reduce the number of free parameters. In Figure 2 we show $L_\alpha^{\mathrm{eff}} - L_w$, determined from

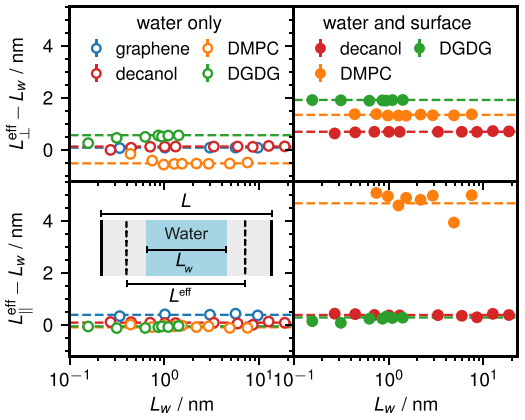

Figure 2. Difference between dielectric width and water slab thickness, $L_\perp^{\mathrm{eff}} - L_w$ (top) and $L_\parallel^{\mathrm{eff}} - L_w$ (bottom), according to eqs 2 and 3, using the SPC/E value $\varepsilon_\alpha^{\mathrm{eff}} = \varepsilon_{\mathrm{bulk}} = 70$. Horizontal dashed lines denote the asymptotic values $\overline{L}_\perp^{\mathrm{eff}} - L_w$ and $\overline{L}_\parallel^{\mathrm{eff}} - L_w$, obtained by averaging the data for $L_w > 1$ nm. The left panels show the water contribution only, and the right panels include the surface polarization contribution.

eqs 2 and 3, as a function of L_w for fixed $\varepsilon_\alpha^{\mathrm{eff}} = \varepsilon_{\mathrm{bulk}} = 70$.[39] The top row shows results for the perpendicular component, the bottom row for the parallel component. In the left panels, we only use the water polarization contribution. In the right panels we use the full polarization including the surface contribution. The differences between the left and right panels indicate the surface contribution to the dielectric response, which is particularly large for the parallel DMPC component (note that there is no surface contribution for our graphene model, and therefore the graphene data are not included in the right figures). Generally, $L_\alpha^{\mathrm{eff}} - L_w$ including the surface polarization contribution is positive, meaning that aqueous interfaces exhibit a positive excess dielectric contribution. As expected, we find that $L_\alpha^{\mathrm{eff}} - L_w$ becomes constant for $L_w > 1$ nm. We thus obtain asymptotic estimates $\overline{L}_\alpha^{\mathrm{eff}} - L_w$ by averaging the data for $L_w > 1$ nm, indicated by broken horizontal lines.

Fixing the effective dielectric constants inside the water slab and determining the effective dielectric widths from simulations, as done in Figure 2, constitute one choice of an effective dielectric model. We now explore an alternative model, where we do not fix the effective dielectric constants. In this case we can derive effective dielectric constants $\varepsilon_\alpha^{\mathrm{eff}}$ in a unique fashion by using the asymptotic effective dielectric widths $\overline{L}_\alpha^{\mathrm{eff}}$ determined in Figure 2. We do this first for graphene because here experimental data exist that we can compare with. Figure 3a shows $\varepsilon_\perp^{\mathrm{eff}}$ according to eq 2 using our graphene simulation data as a function of the graphene layer distance L for different choices of $L_\perp^{\mathrm{eff}}$ (blue spheres). We see that $\varepsilon_\perp^{\mathrm{eff}}$ decreases significantly with rising $L_\perp^{\mathrm{eff}}$, which demonstrates a strong dependence of the effective dielectric constants on the effective dielectric width used. For the asymptotic value $L_\perp^{\mathrm{eff}} = \overline{L}_\perp^{\mathrm{eff}} = L - 0.3$ nm, obtained from $\overline{L}_\perp^{\mathrm{eff}} - L_w = 0.08$ from Figure 2 and $L - L_w = 0.38$ from Supporting

https://dx.doi.org/10.1021/acs.jpcb.0c01967
J. Phys. Chem. B 2020, 124, 4365−4371

The Journal of Physical Chemistry B pubs.acs.org/JPCB Article

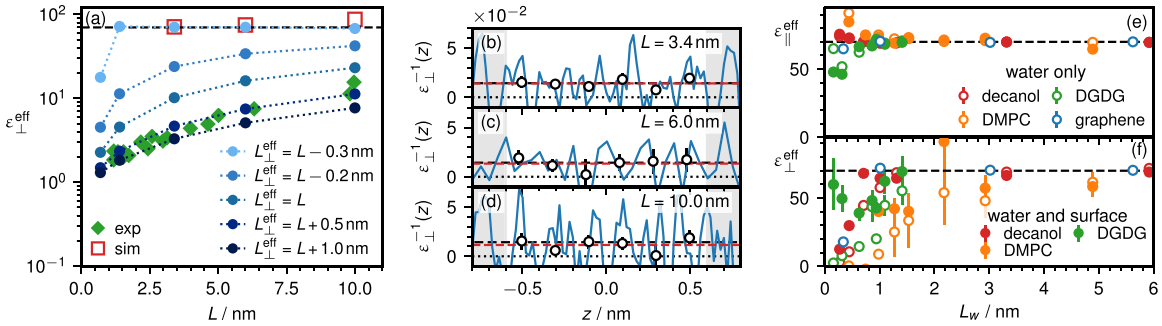

Figure 3. (a) Perpendicular effective dielectric constant $\varepsilon_\perp^{\text{eff}}$ from simulations according to eq 2 for water between graphene sheets as a function of the graphene separation L for different values of the effective dielectric width $L_\perp^{\text{eff}}$ (blue symbols). Open red squares show the dielectric constant directly obtained from averages over the inner region of the graphene system in (b)−(d). Green diamonds show the perpendicular effective dielectric constant from experiments with water between graphene and boron nitride layers using the experimentally employed conversion $L = h + 0.34$ nm, where h is the reported water slab thickness.[30] (b−d) Inverse dielectric profiles $\varepsilon_\perp^{-1}(z)$ from graphene simulations in the slab center for graphene separations L = 3.4, 6.0, 10.0 nm (blue lines). Circles show averages over bins of thickness 0.2 nm, and horizontal red dashed lines denote the average over the central region of thickness 1.2 nm and are in very good agreement with the SPC/E bulk value of $1/\varepsilon_{\text{bulk}} = 1/70$, shown as horizontal black dashed lines. The horizontal black dotted lines denote zero. (e) Parallel effective dielectric constants for all simulated systems according to eq 2 using $\overline{L}_\parallel^{\text{eff}}$ from Figure 2. Open symbols denote the water-only contribution, and full symbols include the surface polarization contribution. (f) Perpendicular effective dielectric constants using $\overline{L}_\perp^{\text{eff}}$ from Figure 2.

Information section S2, we see that the effective dielectric constant stays at its bulk value down to L = 1.4 nm. For the slightly larger value $L_\perp^{\text{eff}} = L$, where the effective dielectric width equals the graphene separation, $\varepsilon_\perp^{\text{eff}}$ is significantly reduced over the entire L range studied. The experimental $\varepsilon_\perp^{\text{eff}}$ for water confined between planar boron nitride and graphene layers, green diamonds, has been obtained by choosing $L_\perp^{\text{eff}} = L - 0.34$ nm in the extraction from the experimental data.[30] It is seen to compare well with our simulations for $L_\perp^{\text{eff}} = L + 0.5$ nm. This shift of $L_\perp^{\text{eff}}$ by 0.84 nm from the scenario where the effective dielectric constant stays at its bulk value down to graphene separation of 1 nm has been interpreted in terms of water interfacial layers with a much reduced dielectric constant[30] (see Supporting Information section S4 for details). It is not clear why these interfacial layers are apparently absent in simulations, which follows from the fact that the simulation data for $L_\perp^{\text{eff}} = \overline{L}_\perp^{\text{eff}} = L - 0.3$ nm differ substantially from the experimental data. One possible explanation could be that the usage of a nonpolarizable force field for the graphene layers produces an unrealistically high water density. However, Figure 2 suggests that surface polarizability increases the interfacial dielectric response and thus would further increase deviations from experiment. In fact, we will next demonstrate how simulations allow unambiguous determination of the correct value of the effective dielectric widths to be used in the extraction of effective dielectric constants.

The simulated values of $\varepsilon_\perp^{\text{eff}}$ in Figure 3a are consistent with experiments only for a specific choice of $L_\perp^{\text{eff}}$, which significantly differs from the value used in the analysis of the experimental data. This prompts the question of what the actual values of $\varepsilon_\perp^{\text{eff}}$ and $\varepsilon_\parallel^{\text{eff}}$ are that should be used in coarse-grained models for confined water slabs. Simulations provide the answer since they can look into the water slab and determine the local dielectric constant, which is model-independent: In Figure 3b−d we show the strongly fluctuating $\varepsilon_\perp^{-1}(z)$ profiles in the central region between graphene at three different separations (blue lines). We also show averages over bins of width 0.2 nm (open spheres) and averages over the inner region of thickness 1.2 nm (red dashed lines), which agree accurately with the SPC/E bulk value $1/\varepsilon_{\text{bulk}} = 0.014$ (black dashed lines). The averages over the inner regions are included in Figure 3a as red squares and agree perfectly with the prediction using the asymptotic dielectric width $L_\perp^{\text{eff}} = \overline{L}_\perp^{\text{eff}} = L - 0.3$ nm. We conclude that only the usage of the asymptotic effective dielectric width $\overline{L}_\perp^{\text{eff}}$ leads to physically sound estimates of effective dielectric constants $\varepsilon_\perp^{\text{eff}}$ and $\varepsilon_\parallel^{\text{eff}}$ that agree with the local dielectric constants in the water slab center. Coming back to the disagreement between the simulation and experimental results in Figure 3a, we mention that this could be explained either by the presence of less water than assumed in the experiments, for example, due to graphene deformation or slow water filling kinetics, or by more water present in the simulations compared to the experiment, for example, due to force field issues.

In Figure 3e and Figure 3f we show the effective dielectric constants $\varepsilon_\parallel^{\text{eff}}$ and $\varepsilon_\perp^{\text{eff}}$ for all four simulated systems using $\overline{L}_\parallel^{\text{eff}}$ and $\overline{L}_\perp^{\text{eff}}$ from Figure 2. We find very little difference between the results excluding (open circles) and including the surface polarization (full circles). The effective parallel dielectric constant $\varepsilon_\parallel^{\text{eff}}$ is rather independent of L_w, while the perpendicular component $\varepsilon_\perp^{\text{eff}}$ decreases significantly below $L_w \approx 1-2$ nm, which has been shown to be due to anticorrelated water dipoles.[29] We conclude that dielectric properties of water are rather independent of the confining medium if the dielectric widths $L_\parallel^{\text{eff}}$ and $L_\perp^{\text{eff}}$ are properly accounted for. As mentioned before, alternatively, one could define an effective model using the bulk dielectric constant of water and employing water-slab-thickness-dependent dielectric widths $\overline{L}_\parallel^{\text{eff}}$ and $\overline{L}_\perp^{\text{eff}}$. So there are different effective dielectric models that describe the same physics.

We now derive effective electrostatic interactions for point-like charges embedded in a linear anisotropic dielectric medium using the effective dielectric constants extracted from simulations. The electrostatic potential $\mathcal{G}(\mathbf{r}, \mathbf{r}')$ created at $\mathbf{r}$ by a unit charge at position $\mathbf{r}'$ follows from Poisson's equation

$$\varepsilon_0\{\nabla[\boldsymbol{\varepsilon}(\mathbf{r})\cdot\nabla\mathcal{G}(\mathbf{r}, \mathbf{r}')]\} = -\delta(\mathbf{r} - \mathbf{r}') \quad (4)$$

https://dx.doi.org/10.1021/acs.jpcb.0c01967
J. Phys. Chem. B 2020, 124, 4365−4371

The Journal of Physical Chemistry B pubs.acs.org/JPCB Article

We assume the diagonal dielectric tensor $\boldsymbol{\varepsilon}(\mathbf{r})$ to be piecewise constant in three spatial regions, as schematically shown in Figure 4. In the Supporting Information section S5 we show

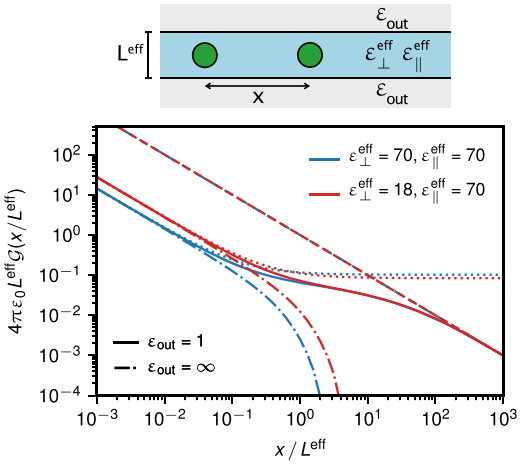

Figure 4. Rescaled electrostatic potential $\mathcal{G}(x/L^{\mathrm{eff}})$ for two charges at a distance x in the water slab center. Solid lines show the exact solution, dotted lines the asymptotic result of eq 5 valid for $x/L^{\mathrm{eff}} \to 0$, dashed lines the asymptotic result of eq 6 valid for $x/L^{\mathrm{eff}} \to \infty$ for a confining vacuum medium ($\varepsilon_{\mathrm{out}} = 1$). Dashed-dotted lines show the exact solution for a confining metallic medium with $\varepsilon_{\mathrm{out}} \to \infty$. All results are presented for two different slab dielectric constants.

that a more detailed model with five regions that accounts for the different effective dielectric widths $L_\parallel^{\mathrm{eff}}$ and $L_\perp^{\mathrm{eff}}$ gives very similar results; we therefore use here $L^{\mathrm{eff}} \equiv L_\parallel^{\mathrm{eff}} = L_\perp^{\mathrm{eff}}$. In Figure 4 we show $\mathcal{G}(x/L^{\mathrm{eff}})$ as a function of the distance x/L^{eff} between two charges positioned in the water slab center. The solid and dashed-dotted lines show results if the outer medium is vacuum ($\varepsilon_{\mathrm{out}} = 1$) and metallic ($\varepsilon_{\mathrm{out}} \to \infty$), respectively. Red lines show results for $\varepsilon_\parallel^{\mathrm{eff}} = 70$ and $\varepsilon_\perp^{\mathrm{eff}} = 18$, representing water between graphene layers at a separation $L = 0.7$ nm (see Figure 3e and Figure 3f), while blue lines are results for $\varepsilon_\parallel^{\mathrm{eff}} = \varepsilon_\perp^{\mathrm{eff}} = 70$, relevant for water between graphene layers that are $L = 1.4$ nm or farther apart (the derivation is detailed in the Supporting Information section S5). The reduction of $\varepsilon_\perp^{\mathrm{eff}}$ significantly enhances electrostatic interactions at low separation, while metallic confinement reduces their range. The dotted lines in Figure 4 show the limiting results for small x,

$$\lim_{x\to 0} \mathcal{G}(x) \simeq \frac{1}{4\pi\varepsilon_0\sqrt{\varepsilon_\perp\varepsilon_\parallel}\,|x|} \tag{5}$$

and the broken lines show the limiting results for large x and outer vacuum medium with $\varepsilon_{\mathrm{out}} = 1$,

$$\lim_{x\to \infty} \mathcal{G}(x) \simeq \frac{1}{4\pi\varepsilon_0\varepsilon_{\mathrm{out}}|x|} \tag{6}$$

Interestingly, eq 5, which describes the interaction accurately for distances below $x/L^{\mathrm{eff}} = 0.5$, depends inversely on the product $\sqrt{\varepsilon_\parallel\varepsilon_\perp}$, which explains why interactions increase at strong confinement where $\varepsilon_\perp$ decreases significantly. For large separations $x/L^{\mathrm{eff}} > 1$ the slab dielectric constants become irrelevant and a slow crossover to eq 6 is observed (in the Supporting Information section S5 a crossover formula is provided, helpful for future coarse-grained simulations). The asymptotic large-distance interaction in metallic confinement with $\varepsilon_{\mathrm{out}} \to \infty$ reads

$$\lim_{x\to\infty} \mathcal{G}(x) \simeq \frac{1}{4\pi\varepsilon_0\varepsilon_\parallel^{3/4}\varepsilon_\perp^{1/4}}\sqrt{\frac{8}{x/L}}\, e^{-\pi\sqrt{\frac{\varepsilon_\perp}{\varepsilon_\parallel}}x/L} \tag{7}$$

and exhibits an exponential decay with a universal decay constant that depends on the ratio $\varepsilon_\parallel^{\mathrm{eff}}/\varepsilon_\perp^{\mathrm{eff}}$, which explains the results in Figure 4 (dashed-dotted lines); see Supporting Information section S5 for derivations of all formulas.

CONCLUSION

We extract dielectric tensorial profiles of confined water from atomistic simulations of four fundamentally different planar systems. Using effective medium theory, we convert dielectric profiles into asymptotic dielectric slab widths and water-slab-thickness dependent effective dielectric constants. Recent experimental measurements of the effective perpendicular dielectric constant of water between graphene and boron-nitride layers[30] can be reproduced if the effective dielectric width used in the extraction is suitably adjusted. Regardless of the system, by choice of values for the effective dielectric widths that follow from our asymptotic analysis for large water slab thicknesses, the parallel effective dielectric constants stay close to the bulk value down to the smallest confinement while the perpendicular effective dielectric constants significantly decrease for confinement below a nanometer. This finding is confirmed by comparison with the local dieletric constant determined in the slab center. An exact solution of the Poisson equation in anisotropic dielectric slabs demonstrates that electrostatic interactions between charges at small separation depend on the product of $\varepsilon_\parallel^{\mathrm{eff}}$ and $\varepsilon_\perp^{\mathrm{eff}}$. If the confining medium is metallic, the charge−charge interactions for large distances decay exponentially with a decay constant that depends on the ratio of $\varepsilon_\parallel^{\mathrm{eff}}$ and $\varepsilon_\perp^{\mathrm{eff}}$. These results not only directly relate to current experiments but also provide the framework for future coarse-grained simulations and theories for electrostatics in aqueous confinement.

ASSOCIATED CONTENT

Supporting Information

The Supporting Information is available free of charge at https://pubs.acs.org/doi/10.1021/acs.jpcb.0c01967.

Simulation details, determination of the effective water slab thickness for graphene system, derivation of the equations for dielectric profiles and dielectric box model, dielectric constant of an effective capacitor model, derivation of the tensorial electrostatic model including limiting cases and a heuristic formula, and correlation time of the total dipole moment in confinement (PDF)

AUTHOR INFORMATION

Corresponding Author

Roland R. Netz − *Fachbereich Physik, Freie Universität Berlin, 14195 Berlin, Germany*; Email: rnetz@physik.fu-berlin.de

Authors

Philip Loche − *Fachbereich Physik, Freie Universität Berlin, 14195 Berlin, Germany*; orcid.org/0000-0002-9112-0010

Cihan Ayaz − *Fachbereich Physik, Freie Universität Berlin, 14195 Berlin, Germany*

https://dx.doi.org/10.1021/acs.jpcb.0c01967
J. Phys. Chem. B 2020, 124, 4365−4371

Amanuel Wolde-Kidan − *Fachbereich Physik, Freie Universität Berlin, 14195 Berlin, Germany*
Alexander Schlaich − *Université Grenoble Alpes, CNRS, LIPhy, 38000 Grenoble, France;* orcid.org/0000-0002-4250-363X

Complete contact information is available at: https://pubs.acs.org/10.1021/acs.jpcb.0c01967

Notes

The authors declare no competing financial interest.

■ ACKNOWLEDGMENTS

The authors acknowledge the Max-Planck Water Initiative for funding and the North-German Supercomputing Alliance (HLRN) for providing HPC resources that have contributed to the research results reported in this paper.

■ REFERENCES

(1) Schoch, R. B.; Han, J.; Renaud, P. Transport phenomena in nanofluidics. *Rev. Mod. Phys.* **2008**, *80*, 839−883.
(2) Bocquet, L.; Charlaix, E. Nanofluidics, from bulk to interfaces. *Chem. Soc. Rev.* **2010**, *39*, 1073−1095.
(3) Geim, A. K.; Grigorieva, I. V. Van der Waals heterostructures. *Nature* **2013**, *499*, 419−425.
(4) Radha, B.; Esfandiar, A.; Wang, F. C.; Rooney, A. P.; Gopinadhan, K.; Keerthi, A.; Mishchenko, A.; Janardanan, A.; Blake, P.; Fumagalli, L.; et al. Molecular transport through capillaries made with atomic-scale precision. *Nature* **2016**, *538*, 222−225.
(5) Gravelle, S.; Yoshida, H.; Joly, L.; Ybert, C.; Bocquet, L. Carbon membranes for efficient water-ethanol separation. *J. Chem. Phys.* **2016**, *145*, 124708.
(6) Hong, S.; Constans, C.; Surmani Martins, M. V.; Seow, Y. C.; Guevara Carrió, J. A.; Garaj, S. Scalable Graphene-Based Membranes for Ionic Sieving with Ultrahigh Charge Selectivity. *Nano Lett.* **2017**, *17*, 728−732.
(7) Zhou, K.-G.; Vasu, K. S.; Cherian, C. T.; Neek-Amal, M.; Zhang, J. C.; Ghorbanfekr-Kalashami, H.; Huang, K.; Marshall, O. P.; Kravets, V. G.; Abraham, J.; et al. Electrically controlled water permeation through graphene oxide membranes. *Nature* **2018**, *559*, 236−240.
(8) Simoncelli, M.; Ganfoud, N.; Sene, A.; Haefele, M.; Daffos, B.; Taberna, P.-L.; Salanne, M.; Simon, P.; Rotenberg, B. Blue Energy and Desalination with Nanoporous Carbon Electrodes: Capacitance from Molecular Simulations to Continuous Models. *Phys. Rev. X* **2018**, *8*, 021024.
(9) Mouterde, T.; Keerthi, A.; Poggioli, A. R.; Dar, S. A.; Siria, A.; Geim, A. K.; Bocquet, L.; Radha, B. Molecular streaming and its voltage control in ångström-scale channels. *Nature* **2019**, *567*, 87−90.
(10) Gopinadhan, K.; Hu, S.; Esfandiar, A.; Lozada-Hidalgo, M.; Wang, F. C.; Yang, Q.; Tyurnina, A. V.; Keerthi, A.; Radha, B.; Geim, A. K. Complete steric exclusion of ions and proton transport through confined monolayer water. *Science* **2019**, *363*, 145−148.
(11) Leikin, S.; Parsegian, V. A.; Rau, D. C.; Rand, R. P. Hydration Forces. *Annu. Rev. Phys. Chem.* **1993**, *44*, 369−395.
(12) Du, Q.; Freysz, E.; Shen, Y. R. Vibrational spectra of water molecules at quartz/water interfaces. *Phys. Rev. Lett.* **1994**, *72*, 238−241.
(13) Maggs, A. C.; Everaers, R. Simulating Nanoscale Dielectric Response. *Phys. Rev. Lett.* **2006**, *96*, 230603.
(14) Li, T.-D.; Gao, J.; Szoszkiewicz, R.; Landman, U.; Riedo, E. Structured and viscous water in subnanometer gaps. *Phys. Rev. B: Condens. Matter Mater. Phys.* **2007**, *75*, 115415.
(15) Snyder, P. W.; Lockett, M. R.; Moustakas, D. T.; Whitesides, G. M. Is it the shape of the cavity, or the shape of the water in the cavity? *Eur. Phys. J.: Spec. Top.* **2014**, *223*, 853−891.
(16) O'Hern, S. C.; Boutilier, M. S. H.; Idrobo, J.-C.; Song, Y.; Kong, J.; Laoui, T.; Atieh, M.; Karnik, R. Selective Ionic Transport through Tunable Subnanometer Pores in Single-Layer Graphene Membranes. *Nano Lett.* **2014**, *14*, 1234−1241.
(17) Jain, T.; Rasera, B. C.; Guerrero, R. J. S.; Boutilier, M. S. H.; O'Hern, S. C.; Idrobo, J.-C.; Karnik, R. Heterogeneous sub-continuum ionic transport in statistically isolated graphene nanopores. *Nat. Nanotechnol.* **2015**, *10*, 1053−1057.
(18) Muñoz-Santiburcio, D.; Marx, D. Chemistry in nanoconfined water. *Chem. Sci.* **2017**, *8*, 3444−3452.
(19) Chakraborty, S.; Kumar, H.; Dasgupta, C.; Maiti, P. K. Confined Water: Structure, Dynamics, and Thermodynamics. *Acc. Chem. Res.* **2017**, *50*, 2139−2146.
(20) Ruiz-Barragan, S.; Muñoz-Santiburcio, D.; Marx, D. Nano-confined Water within Graphene Slit Pores Adopts Distinct Confinement-Dependent Regimes. *J. Phys. Chem. Lett.* **2019**, *10*, 329−334.
(21) Ling, X.; Bonn, M.; Domke, K. F.; Parekh, S. H. Correlated interfacial water transport and proton conductivity in perfluorosulfonic acid membranes. *Proc. Natl. Acad. Sci. U. S. A.* **2019**, *116*, 8715−8720.
(22) Honig, B.; Nicholls, A. Classical electrostatics in biology and chemistry. *Science* **1995**, *268*, 1144−1149.
(23) Ben-Yaakov, D.; Andelman, D.; Podgornik, R. Dielectric decrement as a source of ion-specific effects. *J. Chem. Phys.* **2011**, *134*, 074705.
(24) Bonthuis, D. J.; Gekle, S.; Netz, R. R. Profile of the static permittivity tensor of water at interfaces: consequences for capacitance, hydration interaction and ion adsorption. *Langmuir* **2012**, *28*, 7679−7694.
(25) Stern, H. A.; Feller, S. E. Calculation of the dielectric permittivity profile for a nonuniform system: Application to a lipid bilayer simulation. *J. Chem. Phys.* **2003**, *118*, 3401−3412.
(26) Ballenegger, V.; Hansen, J.-P. Dielectric permittivity profiles of confined polar fluids. *J. Chem. Phys.* **2005**, *122*, 114711.
(27) Cui, H.-B.; Takahashi, K.; Okano, Y.; Kobayashi, H.; Wang, Z.; Kobayashi, A. Dielectric Properties of Porous Molecular Crystals That Contain Polar Molecules. *Angew. Chem., Int. Ed.* **2005**, *44*, 6508−6512.
(28) Zhang, C.; Gygi, F.; Galli, G. Strongly Anisotropic Dielectric Relaxation of Water at the Nanoscale. *J. Phys. Chem. Lett.* **2013**, *4*, 2477−2481.
(29) Schlaich, A.; Knapp, E. W.; Netz, R. R. Water Dielectric Effects in Planar Confinement. *Phys. Rev. Lett.* **2016**, *117*, 048001.
(30) Fumagalli, L.; Esfandiar, A.; Fabregas, R.; Hu, S.; Ares, P.; Janardanan, A.; Yang, Q.; Radha, B.; Taniguchi, T.; Watanabe, K.; et al. Anomalously low dielectric constant of confined water. *Science* **2018**, *360*, 1339−1342.
(31) Ruiz-Barragan, S.; Muñoz-Santiburcio, D.; Körning, S.; Marx, D. Quantifying anisotropic dielectric response properties of nano-confined water within graphene slit pores. *Phys. Chem. Chem. Phys.* **2020**, DOI: 10.1039/D0CP00916D.
(32) Zhang, C. Note: On the dielectric constant of nanoconfined water. *J. Chem. Phys.* **2018**, *148*, 156101.
(33) Hillier, A. C.; Kim, S.; Bard, A. J. Measurement of Double-Layer Forces at the Electrode/Electrolyte Interface Using the Atomic Force Microscope: Potential and Anion Dependent Interactions. *J. Phys. Chem.* **1996**, *100*, 18808−18817.
(34) Rentsch, S.; Siegenthaler, H.; Papastavrou, G. Diffuse Layer Properties of Thiol-Modified Gold Electrodes Probed by Direct Force Measurements. *Langmuir* **2007**, *23*, 9083−9091.
(35) Kanduč, M.; Schneck, E.; Netz, R. R. Hydration Interaction between Phospholipid Membranes: Insight into Different Measurement Ensembles from Atomistic Molecular Dynamics Simulations. *Langmuir* **2013**, *29*, 9126−9137.
(36) Kanduč, M.; Schlaich, A.; de Vries, A. H.; Jouhet, J.; Maréchal, E.; Demé, B.; Netz, R. R.; Schneck, E. Tight cohesion between glycolipid membranes results from balanced water-headgroup interactions. *Nat. Commun.* **2017**, *8*, 14899.
(37) Kornyshev, A. A.; Sutmann, G. Nonlocal Dielectric Saturation in Liquid Water. *Phys. Rev. Lett.* **1997**, *79*, 3435−3438.

(38) Loche, P.; Wolde-Kidan, A.; Schlaich, A.; Bonthuis, D. J.; Netz, R. R. Comment on "Hydrophobic Surface Enhances Electrostatic Interaction in Water. *Phys. Rev. Lett.* **2019**, *123*, 049601.
(39) Vega, C.; Abascal, J. L. F. Simulating water with rigid non-polarizable models: a general perspective. *Phys. Chem. Chem. Phys.* **2011**, *13*, 19663−19688.

https://dx.doi.org/10.1021/acs.jpcb.0c01967
J. Phys. Chem. B 2020, 124, 4365−4371

5

ELECTROSTATICS OF CYLINDRICAL NANO SYSTEMS

Similar to the previous chapter 4, where aqueous systems confined in planar geometry were investigated, drastic changes for the water properties compared to bulk are also expected in cylindrical water-filled channels. Cylindrical channels especially nanotubes are a promising building block for wet nanotechnology and already find widespread use in ultrafiltration [40, 41] and electrokinetic devices [29]. Since ions are present in all of these applications, the correct modeling requires the accurate description of electrostatic ion-ion interactions, which in turn depend on the dielectric properties of water in nanotubes. As we have shown in the last two chapters, the dielectric constant becomes anisotropic at interfaces and in planar confinement.

In this chapter, we determine radial and axial dielectric profiles and from that derive effective dielectric constants of water-filled carbon nanotubes using all-atom molecular dynamics simulations. We find that for nanotube radii below 10 nm, the radial dielectric component reduces significantly while the axial dielectric component exhibits a giant increase. These dielectric properties of nano-tubes arise from confinement and curvature effects, as we show by comparison with simulations of confined water in planar systems and by comparison with an exactly solvable extended Langevin model.

This pronounced anisotropy of the dielectric tensor has profound implications for ion distributions within nanotubes and our results can be directly used in continuum models such as Poisson-Boltzmann's theory. As an explicit application of our results, we use ion-ion interaction via an exact solution of the tensorial Poisson equation in cylindrical geometry previously derived by Ayaz [53]. Quite contrary to intuition, our exact calculation shows that the ion-ion interaction is for small separations dominated by the radial dielectric constant, not the axial one. As a consequence of this, the electrostatic interaction between ions that are arranged axially in a thin water-filled nanotube is enhanced by roughly a factor of 10 compared to the case where the dielectric constant is taken to be that of bulk water. We mention in passing that in all contemporary coarse-grained modeling approaches, the water dielectric constant inside nanotubes is in fact assumed to be isotropic and given by the bulk water value. This ion-ion interaction enhancement significantly modifies the properties of ions in nanotubes with consequences for ion conduction, ion transport and ion chemical equilibria like the protonation/deprotonation equilibria of acids in nanotubes.

DATA AVAILABILITY

The data that support the findings of this chapter are included in the SI of the publication. The simulations are carried out with the 2016 version of the GROMACS simulation package and all analyses are performed with MAICoS. Original simulation and analysis files are available at

http://dx.doi.org/10.17169/refubium-30945.

6

LIMITS OF LINEAR ELECTROSTATICS

Ions at the interface between water and a low-dielectric medium experience an image-charge interaction, repelling them from the interface. This image-charge repulsion has been considered as the ingredient of ion-surface interaction theories since the seminal work by Onsager and Samaras [62]. However, such purely linear electrostatic considerations are insufficient to explain the rich variety of ion adsorption and desorption behavior found in nature, including polymer collapse, DNA condensation, and ion adsorption on solid surfaces [27, 28]. These aspects of the ion-surface interactions have enjoyed a surge in interest in recent years, in particular in the context of graphene interfaces, which can be combined with electrolytes for water desalination [23] and osmotic energy harvesting [25], as well as for the development of so-called supercapacitors [94].

In this chapter, the free energy profile of a chloride ion at a graphene/water interface using all-atom MD simulations is obtained. The free energy is split into electrostatic and Lennard-Jones contributions. Whereas the electrostatic contribution dominates in bulk, we find that the Lennard-Jones contribution exceeds the electrostatic contribution close to the interface. By further examining the electrostatic contribution, we show that non-linear effects are important at surfaces, even for monovalent ions. Applying previously derived Green's function for an anisotropic dielectric tensor [53] we calculate the linear contribution to the electrostatic energy, and accurately reproduce our simulation data without any fitting parameters.

Importantly, our results show that linear electrostatic response theory is insufficient to accurately model ion-surface interactions. Moreover, for the linear contribution to the electrostatic potential, it is essential to take the anisotropy of the dielectric tensor into account. By using the Green's function approach 4 [53] to calculate the electrostatic energy in this situation, we provide the framework for the description of electrostatic interactions at the interface of complex dielectric materials. Furthermore, we conclude that the most accurate way available to model ion-surface interactions is the use of a non-electrostatic contribution to the free energy – extracted from simulations – in the Poisson-Boltzmann equation. Our work explains the physical reasons why this approach, which has become common practice in recent years, is so successful [95–98]. Besides, the fundamental framework for ion interactions at interfaces are easily transferable to other surfaces and even to ion-ion interactions especially in confinement.

DATA AVAILABILITY

The data that support the findings of this chapter are included in the SI of the publication. The simulations are carried out with the 2016 version of the GROMACS simulation package. Original simulation and analysis files are available at

http://dx.doi.org/10.17169/refubium-30946.

7

CONCLUSION

This thesis investigates electrostatic phenomena on the nano scale using classical molecular dynamics simulations and continuum models. Solvation shells around ions are important for physical chemistry, and a combination of MD and thermodynamics is necessary to capture the behavior.

The simulations performed in this thesis are supported by a newly developed ion force field that models the solvation shell around ions with high accuracy. The force field is transferable between different water models and reproduces many properties of electrolytes with higher accuracy compared to previous parametrizations. The final parameters were optimized using the complete parameter space of the Lennard-Jones potential. During the work on this thesis, we continuously optimized the ion parameters. However, due to the long development time for the new consistent ion force, the optimized ion parameters were not used throughout this thesis. However, the parameters of the Cl^- halide applied here are close to the one found at the end of the optimization procedure. A crucial parameter for the agreement of dielectric theory with experiments and simulation is the exact description of the dielectric properties of the liquid close to the interface. We extract dielectric properties of water at a graphene surface, between graphene sheets, decanol monolayers, phospholipid and glycolipid bilayers and carbon nanotubes using extensive molecular dynamics simulations. The simulations show that interfaces break the system isotropy, and therefore the dielectric function in confinement becomes a tensor with two independent components, which are very different from each other. Regardless of the surface type or the geometry, we find that the component parallel to the surface increases for confinement below 2 nm . For cylindrical channels with radii smaller than 1 nm the axial component (parallel to the surface) is massively enhanced, whereas for planar confinement the parallel component is only slightly increased. This suggests that curvature effects play an important role in confinement. Similar curvature effects were previously found also for the water friction coefficient in carbon nanotubes. For the component of the dielectric function perpendicular to the surface, we found that it decreases in planar and cylindrical confinement. In cylindrical confinement the radial component exhibits a much slower crossover as the axial component which can be understood based on an effective capacitor model. Our derived dielectric constants can be employed in any analytical and coarse-grained model to predict the electrostatic interaction between charges at interfaces and confinement.

We extend our simulations by adding one dissolved chloride ion at a single solid graphene interface and extract its electrostatic interaction with the surface using free-energy calculations. The results show that the interaction of the ion with the surface is dominated by the Lennard-Jones contribution and not by Coloumbic contributions. By a further examination of the electrostatic contribution we find that linear response theory breaks down at interfaces if monovalent ions are closer than 1 nm to the surface. Additionally, the linear descriptions of water close to interfaces is also not valid anymore for field strengths above 1.5 V per nm [70]. Field strengths above 1 V per nm are rare but could be either created by externally

applied fields as done in experiments or are naturally present in the vicinity of charged membranes or DNA strands.

Besides the performed simulations we apply a continuum theory for charges in an anisotropic dielectric medium, based on Poisson's equation. This theory can conveniently be used to calculate electrostatic interaction energies and self energies of charges at interfaces and in confinement using our calculated dielectric constants as input. Our theory accurately reproduces the linear part of the free-energy simulations without any fitting parameters. The analytic results also show that ion-ion interactions in confinement are enhanced compared to bulk with consequences for ion conduction and transport as well as for the protonation/deprotonation equilibria of acids.

To put in a nutshell this thesis shows that solvation shells around ions are important for physical chemistry and that a combination of MD and macroscopic thermodynamics is necessary to capture their behavior. In confinement and near interfaces, the combination of solvation shells and surface structures leads to a nonlinear behavior at planar surfaces and anomalous ion-ion interactions in tubes. To capture some of these effects with a continuum theory, the anisotropic dielectric tensor is essential.

8

OUTLOOK

The simulations performed at interfaces and in confinement were not carried out with the newly developed ion force field and modern water models. Rigorous tests of the new parameters at graphene interfaces and carbon nanotubes have already begun. Additionally, hard graphene surfaces, also, only cover a small part of surface types and the established framework of extracting free energies should be extended to other surface types as oil-water and air-water due to their ubiquity in nature for example in atmospheric sciences. Based on preliminary simulation results it is expected that the Lennard-Jones part of the free-energy is not as dominating at soft interfaces compared to the hard graphene investigated here. Additionally, the used graphene surface is hydrophobic and non conducting whereas real graphene has a high conductivity, inducing probable changes in the water structure close to the surface and in the dielectric properties of the liquid. AIMD where the electrons are treated on a quantum level could shed light on this problem.

Another open question is whether some of the salient features seen in experiments of ion and hydronium transport in water channels can be understood based on coarse-grained electrostatic models that utilize Maxwell equations. Therefore, it is indispensable to study simulated ion-ion interactions and compare them to the analytic prediction presented here. As presented here continuum theory is a powerful tool to predict properties of interfacial and confined systems. Although, we also figured out the limits of continuum models. As a consequence of the linear breakdown, the non-linearity of electrostatics and especially also non-electrostatic contribution should be included in novel continuum theories such as Poisson-Boltzmann or the Poisson-Nernst-Planck equation to reasonable predict ionic absorption phenomena or the change of chemical reaction equilibria.

BIBLIOGRAPHY

[1] Xiao-feng Pang. *Water: Molecular Structure And Properties*. World Scientific, 2014. ISBN: 978-981-4440-44-8.

[2] Lydéric Bocquet and Elisabeth Charlaix. « Nanofluidics, from Bulk to Interfaces. » In: *Chemical Society Reviews* (2010). DOI: 10.1039/B909366B.

[3] S Leikin, V A Parsegian, D C Rau, and R P Rand. « Hydration Forces. » In: *Annual Review of Physical Chemistry* (1993). DOI: 10.1146/annurev.pc.44.100193.002101.

[4] Quan Du, Eric Freysz, and Y. Ron Shen. « Vibrational Spectra of Water Molecules at Quartz/Water Interfaces. » In: *Physical Review Letters* (1994). DOI: 10.1103/PhysRevLett.72.238.

[5] A. C. Maggs and R. Everaers. « Simulating Nanoscale Dielectric Response. » In: *Physical Review Letters* (2006). DOI: 10.1103/PhysRevLett.96.230603.

[6] Tai-De Li, Jianping Gao, Robert Szoszkiewicz, Uzi Landman, and Elisa Riedo. « Structured and Viscous Water in Subnanometer Gaps. » In: *Physical Review B* (2007). DOI: 10.1103/PhysRevB.75.115415.

[7] Phillip W. Snyder, Matthew R. Lockett, Demetri T. Moustakas, and George M. Whitesides. « Is It the Shape of the Cavity, or the Shape of the Water in the Cavity? » In: *The European Physical Journal Special Topics* (2014). DOI: 10.1140/epjst/e2013-01818-y.

[8] Sean C. O'Hern, Michael S. H. Boutilier, Juan-Carlos Idrobo, Yi Song, Jing Kong, Tahar Laoui, Muataz Atieh, and Rohit Karnik. « Selective Ionic Transport through Tunable Subnanometer Pores in Single-Layer Graphene Membranes. » In: *Nano Letters* (2014). DOI: 10.1021/nl404118f.

[9] Tarun Jain, Benjamin C. Rasera, Ricardo Jose S. Guerrero, Michael S. H. Boutilier, Sean C. O'Hern, Juan-Carlos Idrobo, and Rohit Karnik. « Heterogeneous Sub-Continuum Ionic Transport in Statistically Isolated Graphene Nanopores. » In: *Nature Nanotechnology* (2015). DOI: 10.1038/nnano.2015.222.

[10] Daniel Muñoz-Santiburcio and Dominik Marx. « Chemistry in Nanoconfined Water. » In: *Chemical Science* (2017). DOI: 10.1039/C6SC04989C.

[11] Sudip Chakraborty, Hemant Kumar, Chandan Dasgupta, and Prabal K. Maiti. « Confined Water: Structure, Dynamics, and Thermodynamics. » In: *Accounts of Chemical Research* (2017). DOI: 10.1021/acs.accounts.6b00617.

[12] Sergi Ruiz-Barragan, Daniel Muñoz-Santiburcio, and Dominik Marx. « Nanoconfined Water within Graphene Slit Pores Adopts Distinct Confinement-Dependent Regimes. » In: *The Journal of Physical Chemistry Letters* (2019). DOI: 10.1021/acs.jpclett.8b03530.

[13] Xiao Ling, Mischa Bonn, Katrin F. Domke, and Sapun H. Parekh. « Correlated Interfacial Water Transport and Proton Conductivity in Perfluorosulfonic Acid Membranes. » In: *Proceedings of the National Academy of Sciences* (2019). DOI: 10.1073/pnas.1817470116.

[14] Reto B. Schoch, Jongyoon Han, and Philippe Renaud. « Transport Phenomena in Nanofluidics. » In: *Reviews of Modern Physics* (2008). DOI: 10.1103/RevModPhys.80.839.

[15] A. K. Geim and I. V. Grigorieva. « Van Der Waals Heterostructures. » In: *Nature* (2013). DOI: 10.1038/nature12385.

[16] B. Radha et al. « Molecular Transport through Capillaries Made with Atomic-Scale Precision. » In: *Nature* (2016). DOI: 10.1038/nature19363.

[17] Simon Gravelle, Hiroaki Yoshida, Laurent Joly, Christophe Ybert, and Lydéric Bocquet. « Carbon Membranes for Efficient Water-Ethanol Separation. » In: *The Journal of Chemical Physics* (2016). DOI: 10.1063/1.4963098.

[18] Seunghyun Hong, Charlotte Constans, Marcos Vinicius Surmani Martins, Yong Chin Seow, Juan Alfredo Guevara Carrió, and Slaven Garaj. « Scalable Graphene-Based Membranes for Ionic Sieving with Ultrahigh Charge Selectivity. » In: *Nano Letters* (2017). DOI: 10.1021/acs.nanolett.6b03837.

[19] K.-G. Zhou et al. « Electrically Controlled Water Permeation through Graphene Oxide Membranes. » In: *Nature* (2018). DOI: 10.1038/s41586-018-0292-y.

[20] Michele Simoncelli, Nidhal Ganfoud, Assane Sene, Matthieu Haefele, Barbara Daffos, Pierre-Louis Taberna, Mathieu Salanne, Patrice Simon, and Benjamin Rotenberg. « Blue Energy and Desalination with Nanoporous Carbon Electrodes: Capacitance from Molecular Simulations to Continuous Models. » In: *Physical Review X* (2018). DOI: 10.1103/PhysRevX.8.021024.

[21] T. Mouterde, A. Keerthi, A. R. Poggioli, S. A. Dar, A. Siria, A. K. Geim, L. Bocquet, and B. Radha. « Molecular Streaming and Its Voltage Control in Ångström-Scale Channels. » In: *Nature* (2019). DOI: 10.1038/s41586-019-0961-5.

[22] K. Gopinadhan, S. Hu, A. Esfandiar, M. Lozada-Hidalgo, F. C. Wang, Q. Yang, A. V. Tyurnina, A. Keerthi, B. Radha, and A. K. Geim. « Complete Steric Exclusion of Ions and Proton Transport through Confined Monolayer Water. » In: *Science* (2019). DOI: 10.1126/science.aau6771.

[23] Liang Chen et al. « Ion Sieving in Graphene Oxide Membranes via Cationic Control of Interlayer Spacing. » In: *Nature* (2017). DOI: 10.1038/nature24044.

[24] L. Fumagalli et al. « Anomalously Low Dielectric Constant of Confined Water. » In: *Science* (2018). DOI: 10.1126/science.aat4191.

[25] Alessandro Siria, Marie-Laure Bocquet, and Lydéric Bocquet. « New Avenues for the Large-Scale Harvesting of Blue Energy. » In: *Nature Reviews Chemistry* (2017).

[26] Rassoul Tabassian, Jung-Hwan Oh, Sooyeun Kim, Donggyu Kim, Seunghwa Ryu, Seung-Min Cho, Nikhil Koratkar, and Il-Kwon Oh. « Graphene-Coated Meshes for Electroactive Flow Control Devices Utilizing Two Antagonistic Functions of Repellency and Permeability. » In: *Nature Communications* (2016). DOI: 10.1038/ncomms13345.

[27] C. Derek Ma, Chenxuan Wang, Claribel Acevedo-Vélez, Samuel H. Gellman, and Nicholas L. Abbott. « Modulation of Hydrophobic Interactions by Proximally Immobilized Ions. » In: *Nature* (2015). DOI: 10.1038/nature14018.

[28] K. Besteman, K. Van Eijk, and S. G. Lemay. « Charge Inversion Accompanies DNA Condensation by Multivalent Ions. » In: *Nature Physics* (2007). DOI: 10.1038/nphys697.

[29] Eleonora Secchi, Antoine Niguès, Laetitia Jubin, Alessandro Siria, and Lydéric Bocquet. « Scaling Behavior for Ionic Transport and Its Fluctuations in Individual Carbon Nanotubes. » In: *Physical Review Letters* (2016). DOI: 10.1103/PhysRevLett.116.154501.

[30] Eleonora Secchi, Sophie Marbach, Antoine Niguès, Derek Stein, Alessandro Siria, and Lydéric Bocquet. « Massive Radius-Dependent Flow Slippage in Carbon Nanotubes. » In: *Nature* (2016). DOI: 10.1038/nature19315.

[31] Yusong Tu, Peng Xiu, Rongzheng Wan, Jun Hu, Ruhong Zhou, and Haiping Fang. « Water-Mediated Signal Multiplication with Y-shaped Carbon Nanotubes. » In: *Proceedings of the National Academy of Sciences* (2009). DOI: 10.1073/pnas.0902676106.

[32] Rohit Karnik, Chuanhua Duan, Kenneth Castelino, Hirofumi Daiguji, and Arun Majumdar. « Rectification of Ionic Current in a Nanofluidic Diode. » In: *Nano Letters* (2007). DOI: 10.1021/nl0628060.

[33] Rohit Karnik, Rong Fan, Min Yue, Deyu Li, Peidong Yang, and Arun Majumdar. « Electrostatic Control of Ions and Molecules in Nanofluidic Transistors. » In: *Nano Letters* (2005). DOI: 10.1021/nl050493b.

[34] Kazuyoshi Murata, Kaoru Mitsuoka, Teruhisa Hirai, Thomas Walz, Peter Agre, J. Bernard Heymann, Andreas Engel, and Yoshinori Fujiyoshi. « Structural Determinants of Water Permeation through Aquaporin-1. » In: *Nature* (2000). DOI: 10.1038/35036519.

[35] Mark S. P. Sansom and Philip C. Biggin. « Biophysics: Water at the Nanoscale. » In: *Nature* (2001). DOI: 10.1038/35102651.

[36] Haixin Sui, Bong-Gyoon Han, John K. Lee, Peter Walian, and Bing K. Jap. « Structural Basis of Water-Specific Transport through the AQP1 Water Channel. » In: *Nature* (2001). DOI: 10.1038/414872a.

[37] Albert L Lehninger, David L Nelson, Michael M Cox, W. H. Freeman and Company, and Macmillan Publishers. *Lehninger Principles of Biochemistry*. New York; Basingstoke: W. H. Freeman and Company : Macmillan Higher Education, 2013. ISBN: 978-1-4641-0962-1 978-1-4292-3414-6.

[38] Ville R. I. Kaila and Gerhard Hummer. « Energetics and Dynamics of Proton Transfer Reactions along Short Water Wires. » In: *Physical chemistry chemical physics: PCCP* (2011). DOI: 10.1039/c1cp21112a.

[39] Yuxing Peng and Gregory A. Voth. « Expanding the View of Proton Pumping in Cytochrome c Oxidase through Computer Simulation. » In: *Biochimica et Biophysica Acta (BBA) - Bioenergetics*. Respiratory Oxidases (2012). DOI: 10.1016/j.bbabio.2011.11.017.

[40] Ben Corry. « Designing Carbon Nanotube Membranes for Efficient Water Desalination. » In: *The Journal of Physical Chemistry B* (2008). DOI: 10.1021/jp709845u.

[41] Mark A. Shannon, Paul W. Bohn, Menachem Elimelech, John G. Georgiadis, Benito J. Mariñas, and Anne M. Mayes. « Science and Technology for Water Purification in the Coming Decades. » In: *Nature* (2008). DOI: 10.1038/nature06599.

[42] Dapeng Cao, Xianren Zhang, Jianfeng Chen, Wenchuan Wang, and Jimmy Yun. « Optimization of Single-Walled Carbon Nanotube Arrays for Methane Storage at Room Temperature. » In: *The Journal of Physical Chemistry B* (2003). DOI: 10.1021/jp036094r.

[43] Massimiliano Bonomi and Carlo Camilloni, eds. *Biomolecular Simulations: Methods and Protocols*. Methods in Molecular Biology. Humana Press, 2019. ISBN: 978-1-4939-9607-0. DOI: 10.1007/978-1-4939-9608-7.

[44] Alexander Schlaich, Bartosz Kowalik, Matej Kanduč, Emanuel Schneck, and Roland R. Netz. « Simulation Techniques for Solvation-Induced Surface-Interactions at Prescribed Water Chemical Potential. » In: *IAS Series, Computational Trends in Solvation and Transport in Liquids*. Forschungszentrum Jülich GmbH, Zentralbibliothek, 52425 Jülich, 2015.

[45] Lalith Perera and Max L. Berkowitz. « Many-body Effects in Molecular Dynamics Simulations of Na+(H2O)n and Cl-(H2O)n Clusters. » In: *The Journal of Chemical Physics* (1991). DOI: 10.1063/1.460992.

[46] Pavel Jungwirth and Douglas J. Tobias. « Specific Ion Effects at the Air/Water Interface. » In: *Chemical Reviews* (2006). DOI: 10.1021/cr0403741.

[47] Zhifeng Jing, Chengwen Liu, Sara Y. Cheng, Rui Qi, Brandon D. Walker, Jean-Philip Piquemal, and Pengyu Ren. « Polarizable Force Fields for Biomolecular Simulations: Recent Advances and Applications. » In: *Annual Review of Biophysics* (2019). DOI: 10.1146/annurev-biophys-070317-033349.

[48] Otto Stern. « Zur Theorie Der Electrolytischen Doppelschicht. » In: *Zeitschrift für Elektrochemie und Angewandte Physikalische Chemie* (1924).

[49] Yuki Uematsu, Roland R. Netz, and Douwe Jan Bonthuis. « Analytical Interfacial Layer Model for the Capacitance and Electrokinetics of Charged Aqueous Interfaces. » In: *Langmuir* (2018). DOI: 10.1021/acs.langmuir.7b04171.

[50] Yuki Uematsu, Roland R. Netz, Lydéric Bocquet, and Douwe Jan Bonthuis. « Crossover of the Power-Law Exponent for Carbon Nanotube Conductivity as a Function of Salinity. » In: *The Journal of Physical Chemistry B* (2018). DOI: 10.1021/acs.jpcb.8b01975.

[51] Douwe Jan Bonthuis and Roland R. Netz. « Beyond the Continuum: How Molecular Solvent Structure Affects Electrostatics and Hydrodynamics at Solid–Electrolyte Interfaces. » In: *The Journal of Physical Chemistry B* (2013). DOI: 10.1021/jp402482q.

[52] Alexander Schlaich, Ernst W. Knapp, and Roland R. Netz. « Water Dielectric Effects in Planar Confinement. » In: *Physical Review Letters* (2016). DOI: 10.1103/PhysRevLett.117.048001.

[53] Cihan Ayaz. « Tensorial Electrostatics in Planar and Cylindrical Geometry. » Unpublished Bachelor's Thesis. Berlin: Freie Universität Berlin, 2016.

[54] Klaus F. Rinne, Stephan Gekle, and Roland R. Netz. « Dissecting Ion-Specific Dielectric Spectra of Sodium-Halide Solutions into Solvation Water and Ionic Contributions. » In: *The Journal of Chemical Physics* (2014). DOI: 10.1063/1.4901927.

[55] Philip Loche, Cihan Ayaz, Alexander Schlaich, Yuki Uematsu, and Roland R. Netz. « Giant Axial Dielectric Response in Water-Filled Nanotubes and Effective Electrostatic Ion–Ion Interactions from a Tensorial Dielectric Model. » In: *The Journal of Physical Chemistry B* (2019). DOI: 10.1021/acs.jpcb.9b09269.

[56] John G. Kirkwood. « Theory of Solutions of Molecules Containing Widely Separated Charges with Special Application to Zwitterions. » In: *The Journal of Chemical Physics* (1934). DOI: 10.1063/1.1749489.

[57] H. Fröhlich. *Theory of Dielectrics: Dielectric Constant and Dielectric Loss.* Oxford University Press, 1987. ISBN: 0-19-851379-8.

[58] John David Jackson. *Classical Electrodynamics Third Edition.* 3 edition. New York: Wiley, 1998. ISBN: 978-0-471-30932-1.

[59] M. Born. « Volumen und Hydratationswärme der Ionen. » In: *Zeitschrift für Physik* (1920). DOI: 10.1007/BF01881023.

[60] Wendell M Latimer, Kennth S. Pitzer, and Cyril M. Slansky. « The Free Energy of Hydration of Gaseous Ions, and the Absolute Potential of the Normal Calomel Electrode. » In: *The Journal of Chemical Physics* (1939). DOI: 10.1063/1.1750387.

[61] David J. Griffiths. *Introduction to Electrodynamics (3rd Edition).* Prentice Hall, 1999. ISBN: 0-13-805326-X.

[62] Lars Onsager and Nicholas N. T. Samaras. « The Surface Tension of Debye-Hückel Electrolytes. » In: *The Journal of Chemical Physics* (1934). DOI: 10.1063/1.1749522.

[63] M. N. Tamashiro and M. A. Constantino. « Ions at the Water-Vapor Interface. » In: *The Journal of Physical Chemistry B* (2010). DOI: 10.1021/jp911898t.

[64] Douwe Jan Bonthuis, Stephan Gekle, and Roland R. Netz. « Profile of the Static Permittivity Tensor of Water at Interfaces: Consequences for Capacitance, Hydration Interaction and Ion Adsorption. » In: *Langmuir: the ACS journal of surfaces and colloids* (2012). DOI: 10.1021/la2051564.

[65] Christian Schaaf and Stephan Gekle. « Dielectric Response of the Water Hydration Layer around Spherical Solutes. » In: *Physical Review E* (2015). DOI: 10.1103/PhysRevE.92.032718.

[66] Cui Zhang, François Gygi, and Giulia Galli. « Strongly Anisotropic Dielectric Relaxation of Water at the Nanoscale. » In: *The Journal of Physical Chemistry Letters* (2013). DOI: 10.1021/jz401108n.

[67] Martin Neumann. « Dipole Moment Fluctuation Formulas in Computer Simulations of Polar Systems. » In: *Molecular Physics* (1983). DOI: 10.1080/00268978300102721.

[68] H. Zhu, A. Ghoufi, A. Szymczyk, B. Balannec, and D. Morineau. « Anomalous Dielectric Behavior of Nanoconfined Electrolytic Solutions. » In: *Phys. Rev. Lett.* (2012). DOI: 10.1103/PhysRevLett.109.107801.

[69] Stephan Gekle and Axel Arnold. « Comment on “Anomalous Dielectric Behavior of Nanoconfined Electrolytic Solutions”. » In: *Physical Review Letters* (2013). DOI: 10.1103/PhysRevLett.111.089801.

[70] Philip Loche, Amanuel Wolde-Kidan, Alexander Schlaich, Douwe Jan Bonthuis, and Roland R. Netz. « Comment on “Hydrophobic Surface Enhances Electrostatic Interaction in Water”. » In: *Physical Review Letters* (2019). DOI: 10.1103/PhysRevLett.123.049601.

[71] V. Ballenegger and J.-P. Hansen. « Dielectric Permittivity Profiles of Confined Polar Fluids. » In: *The Journal of Chemical Physics* (2005). DOI: 10.1063/1.1845431.

[72] Chris Oostenbrink, Alessandra Villa, Alan E. Mark, and Wilfred F. Van Gunsteren. « A Biomolecular Force Field Based on the Free Enthalpy of Hydration and Solvation: The GROMOS Force-Field Parameter Sets 53A5 and 53A6. » In: *Journal of Computational Chemistry* (2004). DOI: 10.1002/jcc.20090.

[73] Junmei Wang, Romain M. Wolf, James W. Caldwell, Peter A. Kollman, and David A. Case. « Development and Testing of a General Amber Force Field. » In: *Journal of Computational Chemistry* (2004). DOI: 10.1002/jcc.20035.

[74] K. Vanommeslaeghe et al. « CHARMM General Force Field: A Force Field for Drug-like Molecules Compatible with the CHARMM All-Atom Additive Biological Force Fields. » In: *Journal of Computational Chemistry* (2010). DOI: 10.1002/jcc.21367.

[75] H. A. Lorentz. « Ueber Die Anwendung Des Satzes Vom Virial in Der Kinetischen Theorie Der Gase. » In: *Annalen der Physik* (1881). DOI: 10.1002/andp.18812480110.

[76] H. A. Bertelot. « Sur Le Mélange Des Gaz. » In: *Comptes rendus hebdomadaires des séances de l'Académie des Sciences* (1898).

[77] Shavkat I. Mamatkulov, Christoph Allolio, Roland R. Netz, and Douwe Jan Bonthuis. « Orientation-Induced Adsorption of Hydrated Protons at the Air–Water Interface. » In: *Angewandte Chemie International Edition* (2017). DOI: 10.1002/anie.201707391.

[78] Ulrich Essmann, Lalith Perera, Max L. Berkowitz, Tom Darden, Hsing Lee, and Lee G. Pedersen. « A Smooth Particle Mesh Ewald Method. » In: *The Journal of Chemical Physics* (1995). DOI: 10.1063/1.470117.

[79] Daan Frenkel and Berend Smit. *Understanding Molecular Simulation, Second Edition: From Algorithms to Applications (Computational Science).* Academic Press, 2001. ISBN: 0-12-267351-4.

[80] H. J. C. Berendsen, J. R. Grigera, and T. P. Straatsma. « The Missing Term in Effective Pair Potentials. » In: *The Journal of Physical Chemistry* (1987). DOI: 10.1021/j100308a038.

[81] Carlos Vega and Jose L. F. Abascal. « Simulating Water with Rigid Non-Polarizable Models: A General Perspective. » In: *Physical Chemistry Chemical Physics* (2011). DOI: 10.1039/C1CP22168J.

[82] Raúl Fuentes-Azcatl and José Alejandre. « Non-Polarizable Force Field of Water Based on the Dielectric Constant: TIP4P/Epsilon. » In: *The Journal of Physical Chemistry B* (2014). DOI: 10.1021/jp410865y.

[83] Thomas E. Cheatham and Peter A. Kollman. « Molecular Dynamics Simulations Highlight the Structural Differences among DNA:DNA, RNA:RNA, and DNA:RNA Hybrid Duplexes. » In: *Journal of the American Chemical Society* (1997). DOI: 10.1021/ja963641w.

[84] Jejoong Yoo and Aleksei Aksimentiev. « Improved Parametrization of Li+, Na+, K+, and Mg2+ Ions for All-Atom Molecular Dynamics Simulations of Nucleic Acid Systems. » In: *The Journal of Physical Chemistry Letters* (2012). DOI: 10.1021/jz201501a.

[85] Christopher C. Valley, Jason D. Perlmutter, Anthony R. Braun, and Jonathan N. Sachs. « NaCl Interactions with Phosphatidylcholine Bilayers Do Not Alter Membrane Structure but Induce Long-Range Ordering of Ions and Water. » In: *The Journal of Membrane Biology* (2011). DOI: 10.1007/s00232-011-9395-1.

[86] Berk Hess and Nico F. A. van der Vegt. « Cation Specific Binding with Protein Surface Charges. » In: *Proceedings of the National Academy of Sciences* (2009). DOI: 10.1073/pnas.0902904106.

[87] Guillaume Lamoureux, Alexander D. MacKerell, and Benoît Roux. « A Simple Polarizable Model of Water Based on Classical Drude Oscillators. » In: *The Journal of Chemical Physics* (2003). DOI: 10.1063/1.1598191.

[88] Miriam Kohagen, Philip E. Mason, and Pavel Jungwirth. « Accounting for Electronic Polarization Effects in Aqueous Sodium Chloride via Molecular Dynamics Aided by Neutron Scattering. » In: *The Journal of Physical Chemistry B* (2016). DOI: 10.1021/acs.jpcb.5b05221.

[89] David E. Smith and Liem X. Dang. « Computer Simulations of NaCl Association in Polarizable Water. » In: *The Journal of Chemical Physics* (1994). DOI: 10.1063/1.466363.

[90] Samantha Weerasinghe and Paul E. Smith. « A Kirkwood–Buff Derived Force Field for Sodium Chloride in Water. » In: *The Journal of Chemical Physics* (2003). DOI: 10.1063/1.1622372.

[91] Maria Fyta and Roland R. Netz. « Ionic Force Field Optimization Based on Single-Ion and Ion-Pair Solvation Properties: Going beyond Standard Mixing Rules. » In: *The Journal of Chemical Physics* (2012). DOI: 10.1063/1.3693330.

[92] Shavkat Mamatkulov, Maria Fyta, and Roland R. Netz. « Force Fields for Divalent Cations Based on Single-Ion and Ion-Pair Properties. » In: *The Journal of Chemical Physics* (2013). DOI: 10.1063/1.4772808.

[93] Douwe Jan Bonthuis, Shavkat I. Mamatkulov, and Roland R. Netz. « Optimization of Classical Nonpolarizable Force Fields for OH- and H3O+. » In: *The Journal of Chemical Physics* (2016). DOI: 10.1063/1.4942771.

[94] Guang Feng, Song Li, Volker Presser, and Peter T. Cummings. « Molecular Insights into Carbon Supercapacitors Based on Room-Temperature Ionic Liquids. » In: *The Journal of Physical Chemistry Letters* (2013). DOI: 10.1021/jz4014163.

[95] Guangming Luo, Sarka Malkova, Jaesung Yoon, David G. Schultz, Binhua Lin, Mati Meron, Ilan Benjamin, Petr Vanýsek, and Mark L. Schlossman. « Ion Distributions near a Liquid-Liquid Interface. » In: *Science* (2006). DOI: 10.1126/science.1120392.

[96] Dominik Horinek, Andreas Serr, Douwe Jan Bonthuis, Mathias Boström, Werner Kunz, and Roland R. Netz. « Molecular Hydrophobic Attraction and Ion-Specific Effects Studied by Molecular Dynamics. » In: *Langmuir* (2008). DOI: 10.1021/la702485r.

[97] Nadine Schwierz and Roland R. Netz. « Effective Interaction between Two Ion-Adsorbing Plates: Hofmeister Series and Salting-In/Salting-Out Phase Diagrams from a Global Mean-Field Analysis. » In: *Langmuir* (2012). DOI: 10.1021/la204060k.

[98] Yuki Uematsu, Douwe Jan Bonthuis, and Roland R. Netz. « Charged Surface-Active Impurities at Nanomolar Concentration Induce Jones–Ray Effect. » In: *The Journal of Physical Chemistry Letters* (2018). DOI: 10.1021/acs.jpclett.7b02960.

ADDENDUM

Besides all the scientific outcomes of a Ph.D. thesis, documented in publications or inside the thesis itself there are several « behind the scenes aspects » that usually are not covered. In the following, I will focus on two aspects especially relevant in numerical works. Intensive works in computational science require strong computers requiring a lot of energy and additionally effective number-crunching also relies upon powerful programs.

In my case, the latter boils down to a fast simulation package and clever analysis scripts. My work relied on two major open-source libraries where I also contributed code to improve these package: first GROMACS - the MD package I used for running all simulation throughout this thesis and MDAnalysis - A Python library used to analyze MD trajectories. Based on MDAnalysis we developed our own library called MAICoS - Molecular Analysis for Interfacial and Confined Systems - which already is used by other scientists. Summing up at least 17937 lines of code were newly written or changed during the work on this thesis, which was probably the most time-consuming part during the last four years. The number is calculated based on statistics made available by version control systems, like Github and Gitlab.

In addition to writing code, running numerical projects depends on strong computers. These machines located at high-performance clusters at the department and at the Freie Universität Berlin require a lot of electrical power. Since we are living in a century where climate change is one of the most fundamental problems to be solved by humanity it is reasonable to raise awareness of the climate resources necessary for scientific work. If not even scientists are aware of their climate footprint, how can we demand responsibility from everybody? The table on the bottom of the page shows the energy consumption and the emitted CO_2 equivalent based on the average emission of the German electric power generation in 2019 (0.401 kg per kWh). Even though the Freie Universität is purchasing CO_2-neutral electricity, it is worth calculating the emissions based on the countrywide average. The calculation of the energy consumption is based on the thermal design power given by the manufacturers of the CPUs and GPUs. The calculation only contains generated data that ended up in the publications. Prototyping, which in practice, takes most of the simulation time was not taken into account. The total CO_2-emission of my four-year thesis is a bit less compared to the 9440 kg of annual German CO_2 emission per capita. Most of the energy was necessary for the first and the last chapter where the numerically expensive methods for calculating free energies were applied.

CHAPTER	ENERGY CONSUMPTION (KWH)	CO_2-EMISSION (KG)
3	3803	1525
4	1707	684
5	1817	729
6	10333	4144
Total	17660	7082

ACKNOWLEDGMENTS

First of all, let me thank **Roland Netz** for allowing me to work in his group. During the time already starting within my Master's, I always had a lot of freedom for bringing my thoughts into our common projects, while I also had the liberty of working on my ideas. During our sometimes long but always fruitful discussions, he was a critical referee of our work, but he never lost his kindness, and we often ended up chatting about sports, food, or other things far away from physics. In addition, I always enjoyed the relaxed working atmosphere and the wonderful colleagues in the group, who always helped each other with problems leading to a very productive time for me.

Furthermore, I would like to thank **Douwe Bonthuis**, who was a postdoc in our group and now is one of my closest collaborators. In the numerous discussions he always helped in moving projects further, having new solutions when I was puzzled, **Alexander Schlaich** for his caring support during my Master's and as well during my graduation. He taught me the mathematical and computational basics of this work and became a close friend. With **Cihan Ayaz** I spent uncountable hours in front of the blackboard, and only due to his outstanding analytical skills we figured out some of the results presented here.

The results of this thesis would also not possible without the marvelous work of the department's IT staff. Especially, **Jens Dreger** and **Jörg Behrmann** helped me with the encountered IT problems and always had another powerful machine in their shelves when there was not enough computational power available.

I furthermore thank our secretary **Annette Schumann-Welde** and the best desk neighbor **Laura Lavacchi**. Countless acknowledgments also go to **Marcel Goihl**, **Daniel Litinksi**, **Till Kolster** and **Nikolai Passler** for the great time we spent together during our study at the department, solving tasks that where unsolvable on the first glance. I'm also grateful to **Anna Lebowsky**, **Alexander Rathert** and **Olof Peters** for proofreading and their insightful comments on this thesis.

Special thanks also go to **Sibylle "Billy" Meimberg**, and to the nature of Valentinswerder, where I spent most of the time finishing this work. Lastly, I wish to thank **my family** and all the unlisted **friends** for their unlimited support and understanding.

SELBSTSTÄNDIGKEITSERKLÄRUNG

Ich erkläre gegenüber der Freien Universität Berlin, dass ich die vorliegende Dissertation selbstständig und ohne Benutzung anderer als der angegebenen Quellen und Hilfsmittel angefertigt habe. Die vorliegende Arbeit ist frei von Plagiaten. Alle Ausführungen, die wörtlich oder inhaltlich aus anderen Schriften entnommen sind, habe ich als solche kenntlich gemacht. Diese Dissertation wurde in gleicher oder ähnlicher Form noch in keinem früheren Promotionsverfahren eingereicht.

Mit einer Prüfung meiner Arbeit durch ein Plagiatsprüfungsprogramm erkläre ich mich einverstanden.

Berlin, 14.07.2021

Philip Loche

COLOPHON

This thesis was typeset with LaTeX and the typographical layout `classicthesis` developed by André Miede and Ivo Pletikosić.

The *Linux Libertine* digital typeface created by the 'Libertine Open Fonts Project licensed under the GNU General Public License and the SIL Open Font License are used.

Final Version as of January 1, 2022 (1.0).